

Article

Vibration Attenuation in a High-Rise Hybrid-Timber Building: A Comparative Study

Suvash Chapain¹ and Aly Mousaad Aly^{1,2,*} 

¹ Windstorm Impact, Science & Engineering (WISE) Research Lab, Louisiana State University, 3230 H Patrick F. Taylor Hall, Baton Rouge, LA 70803, USA

² O.H. Hinsdale Wave Research Laboratory, School of Civil and Construction Engineering, Oregon State University, 3550 SW Jefferson Way, Corvallis, OR 97331, USA

* Correspondence: aly@lsu.edu

Abstract: Recent developments in engineered timber products, and their availability, durability, and renewability, have led to taller and more flexible buildings. However, these buildings may experience excessive vibrations, resulting in safety and serviceability issues due to wind or earthquake loads. This paper presents a dynamic analysis of a 42-story-tall hybrid-timber building, along with a comparative study of the performance of three damping devices: (i) pendulum pounding tuned mass damper (PTMD), (ii) tuned mass damper inerter (TMDI), and (iii) tuned mass damper (TMD). First, we evaluate the vibration reduction capability of the TMD and the TMDI under filtered white noise and variable frequency sinusoidal excitations. Then, we propose a robust pendulum PTMD designed using the Hertz contact law to minimize the responses under seismic excitations. For a fair comparison, the mass of the TMD, TMDI, and pendulum PTMD is kept the same. The results show that the pendulum PTMD has higher performance and can reduce the peak accelerations under earthquake loads when both TMD and TMDI fail to achieve this requirement. The superior performance of the proposed device in reducing peak accelerations relates to the reduction in damage to structural and nonstructural components under seismic loads. Nevertheless, coupling the inerter and TMD to form a TMDI may shift the optimum frequency and damping ratios, leading to reduced performance. Compared to TMD and TMDI, the proposed pendulum PTMD is more robust, with higher performance in reducing the base shear (55.7%), base moment (41%), and inter-story drift ratio (40%). The dominant capabilities of this novel device in a timber-hybrid building under different excitations reveal benefits that can shape the future of the physical infrastructure and contribute to climate change adaptation and mitigation for improved disaster resilience and circular economy policies.

Keywords: tuned mass damper (TMD); pendulum pounding TMD; TMD inerter; vibration control; dynamics; timber buildings; high-ris



Citation: Chapain, S.; Aly, A.M. Vibration Attenuation in a High-Rise Hybrid-Timber Building: A Comparative Study. *Appl. Sci.* **2023**, *13*, 2230. <https://doi.org/10.3390/app13042230>

Academic Editor: Mahmoud Bayat

Received: 26 December 2022

Revised: 3 February 2023

Accepted: 5 February 2023

Published: 9 February 2023



Copyright: © 2023 by the authors. Licensee MDPI, Basel, Switzerland. This article is an open access article distributed under the terms and conditions of the Creative Commons Attribution (CC BY) license (<https://creativecommons.org/licenses/by/4.0/>).

1. Introduction

Solid timber constructions are a potential replacement for steel and concrete, offering economic viability and environmental sustainability. In addition, timber buildings can reserve carbon throughout their lifecycle and minimize greenhouse emissions. Over the past decade, the development of engineered timber products like cross-laminated timber (CLT) and glue-laminated timber made it possible to construct high-rise buildings. CLT is suitable for floor diaphragms and shear walls. The nine-story residential building Stadthaus, built in London in 2009, is considered one of the first tall timber buildings where CLT is used as a structural material. The global trend of high-rise timber/timber-hybrid worldwide is shown in Table 1 [1]. Other timber high-rise buildings, such as the Terrace House in Vancouver, Canada, and the HoHo Wien in Vienna, Germany, are under construction.

Table 1. Trend of timber/timber-hybrid building in the world.

Building Name	Height (m)	Year Completed	Country
Stadthaus	29 m	2007	United Kingdom
Life Cycle Tower	27 m	2012	Austria
Forte	32 m	2012	Australia
Treet	49 m	2014	Norway
Brock Common UBC	53 m	2017	Canada
Mjøstårnet	85 m	2019	Norway
Ascent MKE	87 m	2022	United States of America

The research on tall mass-timber buildings has been gaining strong momentum, and several countries are developing their codes and guidelines. However, there is a lack of standards and regulations to fully address the expanded application of engineered timber products and timber composite in the construction of buildings. Future trends in timber construction should focus on the research and development of mass timber and hybrid structures, innovative connection designs, timber composites, and retrofitting existing buildings with the timber [2]. Over the past few decades, a notable amount of research has been performed to investigate the wind and earthquake impacts on low-rise timber buildings. Less significant effort has been devoted to studying the dynamic performance of tall timber buildings [3–7].

Timber-Based Hybridization

Even though timber buildings have existed for several years, few high-rise structures are made of pure wood because of construction limitations. From a structural point of view, one of the most significant limitations is that timber is brittle when acted upon by tensile and shear forces. Under seismic loadings, timber may exhibit non-ductile failure that does not dissipate enough energy and can result in disastrous loss. Because of the lack of ductility in seismic design, less self-weight to resist overturning forces imposed by seismic and wind loads, and the possible loss of stiffness under cyclic loadings, mass timber designs consider timber-based hybrid solutions. Timber-based hybrid structures combine timber with other materials, increasing timber's application beyond the current limitations. Most existing timber buildings are hybrid because usually, the connections are steel, and the foundation is concrete. Hybridization is the method that combines two or more different materials by forming a single system in which the advantage of each material is enhanced, and the shortcomings are reduced [8]. Hybridization is divided into two types: component hybridization and system hybridization. In component hybridization, two distinct materials are blended to form a single structural element, such as a hybrid beam, column, or bridge deck. Still, different structural elements are combined in system hybridization to share the load acting on them [9]. Timber-based hybrid structures have been built without clear guidelines based on conservative design assumptions.

Nonetheless, the introduction of force-based seismic design, strength reduction factor, ductility reduction factor, and fundamental period of hybrid structures are of prime importance [10]. Furthermore, structural damping improves performance, enhances safety, and reduces wind-induced fatigue loads [11]. Nonetheless, due to a lack of research efforts and full-scale data, the performance of tall mass timber buildings under dynamic loads has not been well understood [12,13].

Tuned mass damper (TMD) has been studied extensively in the past few decades, and those devices have been installed in many tall buildings around the world to reduce the vibration under wind load. However, the seismic performance of TMD in a tall building is poor and could worsen the structural responses if the excitation frequency is far from the tuning frequency [14,15]. Recently, modified versions of TMD have been studied extensively to find an optimal solution for multiple hazard loads (wind and earthquake). One modified version is a tuned mass damper inerter (TMDI), formed by introducing

an inerter in classical TMD. Previous research has shown that the inerter could virtually increase the mass of TMD to reduce the structural response.

In contrast, pendulum pounding tuned mass damper (PTMD) is formed by introducing the viscous material at the boundary of TMD to dissipate vibration energy. This device has also been studied extensively in recent years. The current study presents the dynamic analysis of a tall hybrid-timber building under filtered white noise, variable frequency sinusoidal, and seismic excitations. In addition, a comparative performance study of three control devices (TMD, TMDI, and pendulum PTMD) is conducted to understand their performance in reducing excessive vibrations in a 42-story hybrid-timber building.

The paper presents computational research to advance the fundamental understanding of coupled multi-physics, multi-functional behavior of hybrid-timber buildings. Section 2 offers a brief review of multi-hazard impacts on tall timber buildings. Section 3 describes the physical and dynamic properties of the case study of a 42-story mass hybrid-timber building. In Section 4, the working principle of the TMDI is presented, and the equivalent TMD is proposed by considering the physical mass of the inerter. The modeling of the case study building equipped with TMDI and TMD is presented in Section 5. In Section 6, numerical optimization of both TMDI and equivalent TMD is conducted under filtered white noise and variable frequency excitations. Section 7 introduces a robust pendulum PTMD with particular emphasis on the pounding force model. A performance-based comparison among TMDI, equivalent TMD, and the pendulum PTMD under fundamental earthquake excitations is presented in Section 8. Finally, the findings of this study are articulated in Section 9.

2. Wind and Earthquake Performance of Timber Buildings

2.1. Seismic Performance

The seismic performance of tall buildings made of concrete/steel has been studied for decades [16,17]. However, there is limited research to understand the seismic behavior of tall timber buildings. Therefore, it is essential to grasp the performance of the CLT under earthquakes to understand the seismic behavior of the timber building. A critical issue in seismic design is identifying the suitable ductile failure mechanism. The seismic design allows inelastic action in a predefined ductile zone for energy dissipation within the structural system. Because timber has limitations under tension/shear forces, steel connections provide ductility in timber structures. For mass-timber buildings, most ductile failure is a shear failure in nailed connections. Other connections are usually brittle and should be strengthened [18,19]. Numerous experimental and analytical studies have been carried out to understand the seismic performance of the CLT wall system [20–24].

The 'SOFIE—Sistema Costruttivo Fiemme's project' in Europe has performed several experimental studies, from a CLT wall to a seven-story timber building to develop seismic resilient mass timber buildings. A CLT building subjected to five different earthquakes shows that the sliding and rocking deformation of the wall panel causes the failure of nails in the bracket on the first floor. The inter-story drift ratio was 3.2%, suggesting that the CLT wall can survive significant deformation [25]. Researchers in the SOFIE project first performed a pseudo-dynamic test of a one-story timber building made up of CLT in the shake table. Then, another shake table test was performed on a three-story building by applying ground acceleration in a single direction. Finally, in 2007, a seven-story mass timber building was tested using ground acceleration in all three directions. The finding of the full-scale test showed that the building could survive without significant lateral deformation under a series of high-intensity earthquakes. However, damage in the connections, angle brackets, and fastener was observed, suggesting that damage was repairable and the CLT wall remained intact [24]. Considerable numbers of innovative connections have been proposed recently for the better performance of timber buildings against earthquakes. From previous studies, it has been observed that stiffness characteristics of joints in timber structures depend upon the load duration and maximum load experienced by the joints. This observation suggests that the dynamic behavior of

the timber structure may vary throughout its lifetime. Thus, care must be taken in the design to gauge the structural responses at all stages of its design life [26]. Nevertheless, most previous studies mainly focused on low-rise to mid-rise buildings with limited knowledge about how tall mass-timber buildings can perform against earthquakes. As there is a growing trend of larger, taller, and more complex mass timber buildings, a detailed understanding of the mechanical features of the connection system will be required [2].

2.2. Wind Performance

Most research has focused on timber as a structural material, fire safety, and seismic performance; however, less research has been focused on evaluating the wind impacts on tall mass timber buildings [27]. Timber high-rise buildings are often lightweight and flexible compared to concrete and steel buildings. Due to higher flexibility, tall timber buildings are more susceptible to the excessive vibrations induced by high wind. Excessive vibration caused by wind loads in tall timber buildings may result in discomfort to the inhabitants, which could endanger the serviceability as well as the economic viability of the structure. Similarly, seismic impact on multi-story timber buildings can cause structural and nonstructural damage. Due to the excellent weight-to-stiffness ratio and ductility of timber, mass-timber buildings represent an attractive solution in seismic areas. However, their serviceability under wind loading is a challenge [24].

The effectiveness of high-rise timber buildings under tornado-like wind fields has been presented in Ref. [28]. Wind tunnel tests and dynamic analysis were conducted to assess the various levels of damage caused by a tornado. A strong tornado can cause damage to drift-sensitive nonstructural elements in tall timber buildings. A study of wind-induced vibrations in a 22-story mass timber building was done where the impact of the dynamic properties of the building was evaluated. The results showed that it is crucial to consider wind-induced vibrations of mass timber buildings for occupant comfort [29]. Recently, a reliability approach has been utilized to evaluate the wind impact on tall timber buildings, including several uncertainties associated with loads. Generally, damping in timber buildings is considered higher than in identical buildings made of concrete and steel because the connections in timber buildings dissipate a higher amount of energy even at the service level. However, there is a lack of advancement in defining sources and mechanisms of inherent damping in tall timber buildings. Seismic analysis of the timber-hybrid should be performed using a nonlinear approach for precise results; however, this is often not feasible due to time and calculation costs. Some efforts have been made to reduce the cost of nonlinear analysis, such as the proposed discrete wave transform method [30].

3. Case Study of a Mass Timber Building

A 42-story tall timber building with a height of 120 m and a cross-section of 36 m × 21 m is considered in the current study. The conceptual structural system of the building is based on an existing reinforced concrete structure (Dewitt-Chestnut Apartments, in Chicago) designed by SOM LLP [31]. Mass timber products CLT and glulam are used for floors, shear walls, and columns, whereas the beams are reinforced concrete. The primary structural system consists of mass timber products with reinforced concrete in highly stressed regions such as joints and foundations. The resulting structural design is considered competitive with concrete and steel buildings while reducing the carbon footprint by approximately 70%. The floor consists of the CLT plates that span between concrete spandrel beams and glue-laminated timber columns. It has a flat plate system like a concrete floor, where panels are restrained at the columns and walls through the reinforcement. A 3-dimensional prospect of the building is presented in Figure 1.

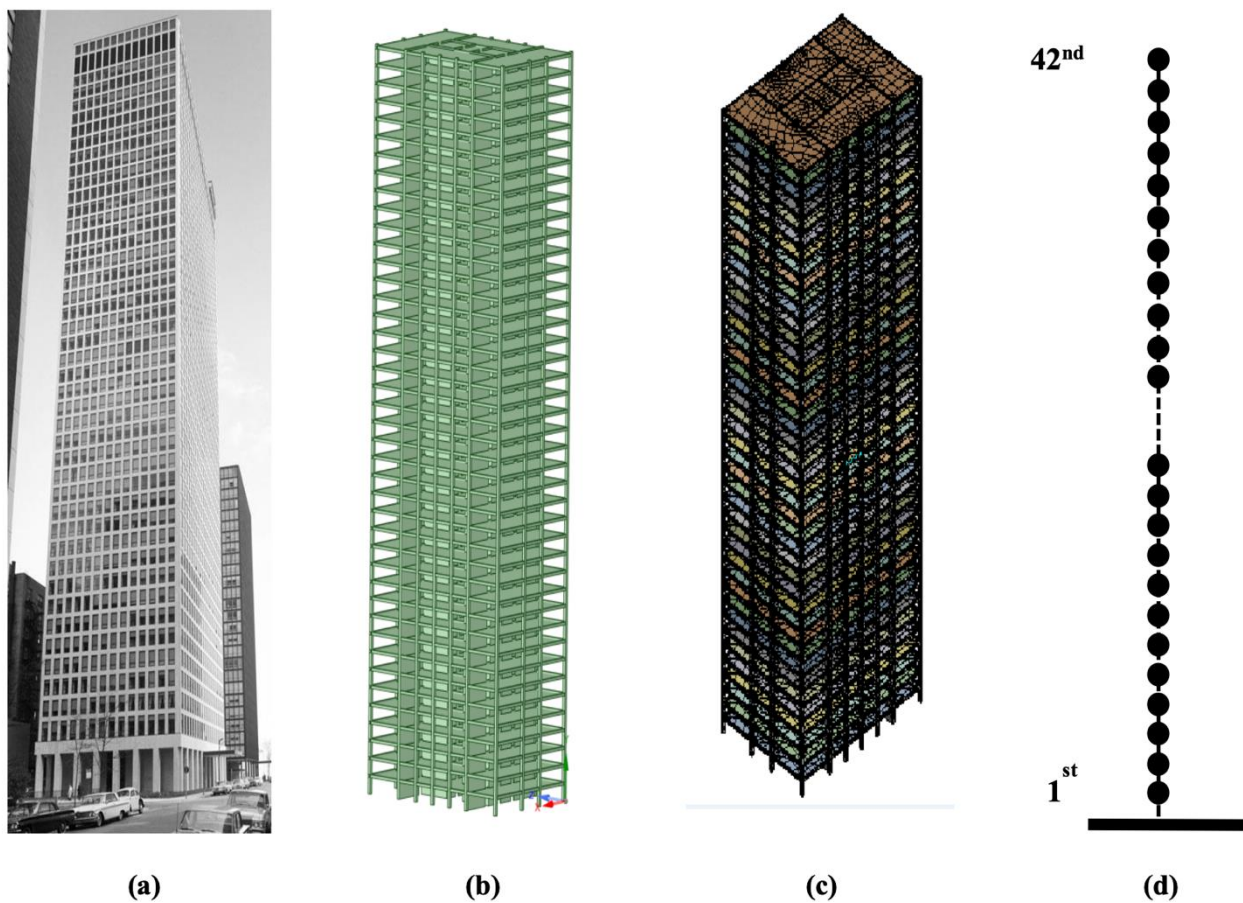


Figure 1. The case study hybrid-timber building: (a) DeWitt Chestnut apartments, Chicago, (b) FEM of proposed timber building, (c) meshing in ANSYS, and (d) lumped mass model.

Gravity load resisting system: The design of the CLT floor is governed by either out-of-plane bending demand imposed by gravity loads or threshold of structural vibration. In this study, the out-of-plane bending strength of the CLT floor was evaluated from the provisions of the American Wood Council [32]. Based on demand, seven layers of CLT were considered for the floor. Highly stressed perimeter columns with a size of 40×40 inches and nine smaller square shape glulam columns were considered. Perimeter columns were designed to withstand gravity load demands. The capacity of those columns was calculated using standard provisions by considering elastic buckling and size effect [32].

Lateral load resisting system: Wind load acting on the building transfers through the floor diaphragm and is opposed by coupled action of core walls and CLT shear walls. The concrete link connects the CLT shear wall and core wall beams so that the entire building acts as a shear flexure cantilever [33]. Shear walls are positioned around the center of the building, forming a sizeable tube-like structure to resist the uplift from the wind loads from both directions. The extra shear wall extends from the core to the perimeter column in both directions (see Figure 2 for details) [27,31]. The Holz–Stahl–Komposit (HSK) system links the CLT floors and walls with spandrel beams [34]. Capacity design principles have been used for the lateral load-resisting system. Under seismic or extreme wind loads, three stages of progressive failure will happen: first, the inelastic rotation will occur on the reinforced concrete link beam; next, the HSK connector will yield; finally, wood crushing could occur at the corner of the CLT walls.

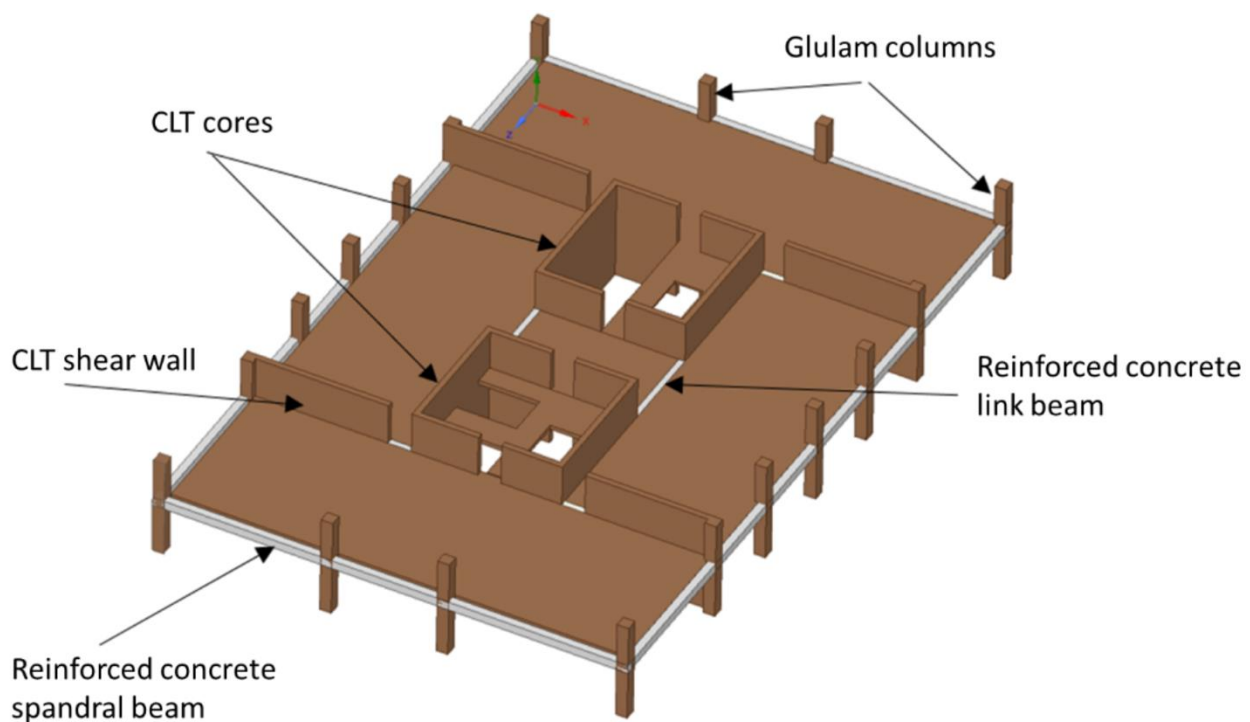


Figure 2. 3D schematic view of a typical floor.

The building's finite element model (FEM) is developed using ANSYS to predict the structure's response under multi-hazard impacts. To produce the model's slabs, shear walls, and cores are represented by plate and beam elements for beams and columns. A three-dimensional model of a mass timber building is shown in Figure 2, where the properties of structural elements are obtained using the CLT handbook [35]. The first six natural frequencies of the buildings are 0.3896 Hz, 0.4229 Hz, 0.7948 Hz, 1.466 Hz, 1.699 Hz, and 1.963 Hz, respectively. Next, the mass of each story, including structural and nonstructural elements, is calculated using Ref. [35]. The total mass of the building is 2.43×10^7 kg, which is distributed along with the height of the building. The model consists of 95,842 elements and 362,827 nodes.

Figure 3 shows the mode shapes of the building for the first six modes. This building behaves like a combination of shear action and bending action. Although natural frequencies and mode shapes of the buildings are obtained through FEM, there is no convincing way to calculate the amount of inherent damping in the building because it depends on several parameters, such as friction between joints and hysteretic characteristics of the material. However, there have been some efforts to predict structural damping based on previous full-scale observations. For example, Tamura and Yoshida proposed one of the widely accepted formulas to predict the structural damping of tall buildings for the first mode [36], where building height and roof displacement are considered parameters. As a result, the inherent damping ratio of the tall building is given as follows:

$$\zeta = \frac{0.93}{H} + 470 \frac{x_H}{H} - 0.0018 \quad (1)$$

where H is the building height, and x_H is the displacement at the top of the buildings. This equation is usually used for concrete buildings, and there have not been many studies on mass timber buildings and their damping. Thus, a damping ratio of 1% is considered for this building. Once natural frequencies, mode shapes, and damping are known, the building's response under wind loads can be obtained using the pressure integration technique [37]. In the next step, the lumped mass system is built to represent the tall building, keeping in mind that the mass is concentrated at each floor and stiffness is located

between the adjacent floors. The lumped mass system represents a full-scale building where the dynamic properties of the structures are made approximately identical. Therefore, all the dynamic properties of the building are reflected in the lumped mass system.

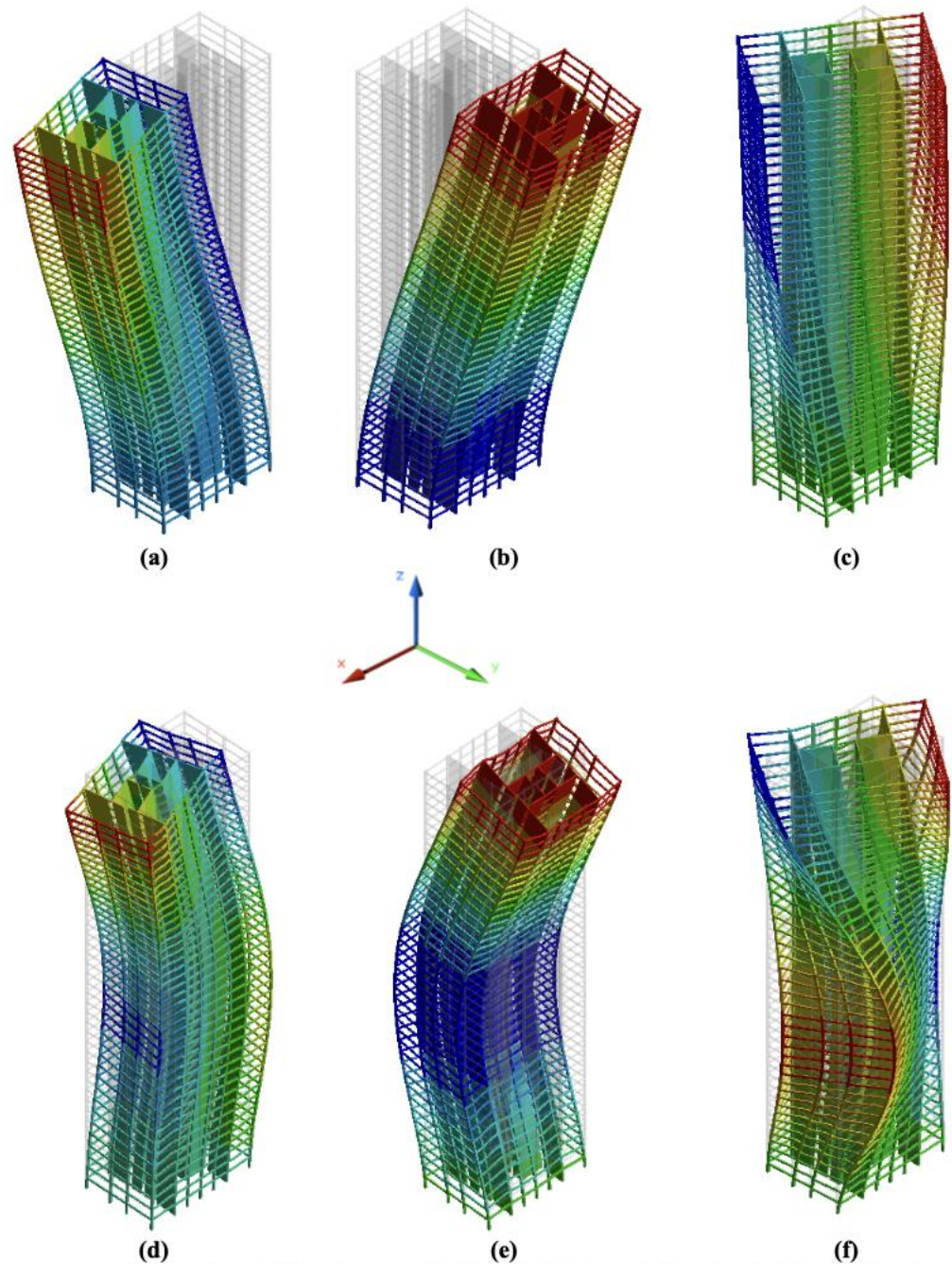


Figure 3. Mode shapes from the finite element model: (a) mode 1 (0.3896 Hz), (b) mode 2 (0.4229 Hz), (c) mode 3 (0.7948 Hz), (d) mode 4 (1.466 Hz), (e) mode 5 (1.699 Hz), and (f) mode 6 (1.963 Hz).

Figure 4 shows a mode shape comparison between the finite element model and the lumped mass system in the x-direction. The stiffness matrix was derived using MATLAB codes so that mode shapes and natural frequencies are close to those from the FEM, at least for the first few modes, as shown in Figure 4. The first mode shape from the FEM matches the lumped mass model by 99%; similarly, the second mode is 95% accurate, while the third mode is 85% accurate. The first natural frequency matches 100% with the FEM model, while other modal frequencies have slight variations. A comparison of natural frequencies

between the FEM and lumped mass model is shown in Table 2. The whole idea of this comparison is to capture the dynamic properties of the designed mass-timber building in the lumped mass system. After deriving the mass and stiffness matrices, the damping matrix \mathbf{C} is derived using equivalent Rayleigh damping [38].

$$\mathbf{C} = \alpha\mathbf{M} + \beta\mathbf{K} \quad (2)$$

where \mathbf{M} is the mass matrix and \mathbf{K} is the stiffness matrix obtained as a combination of shear and cantilever action. Both α and β are predefined constants.

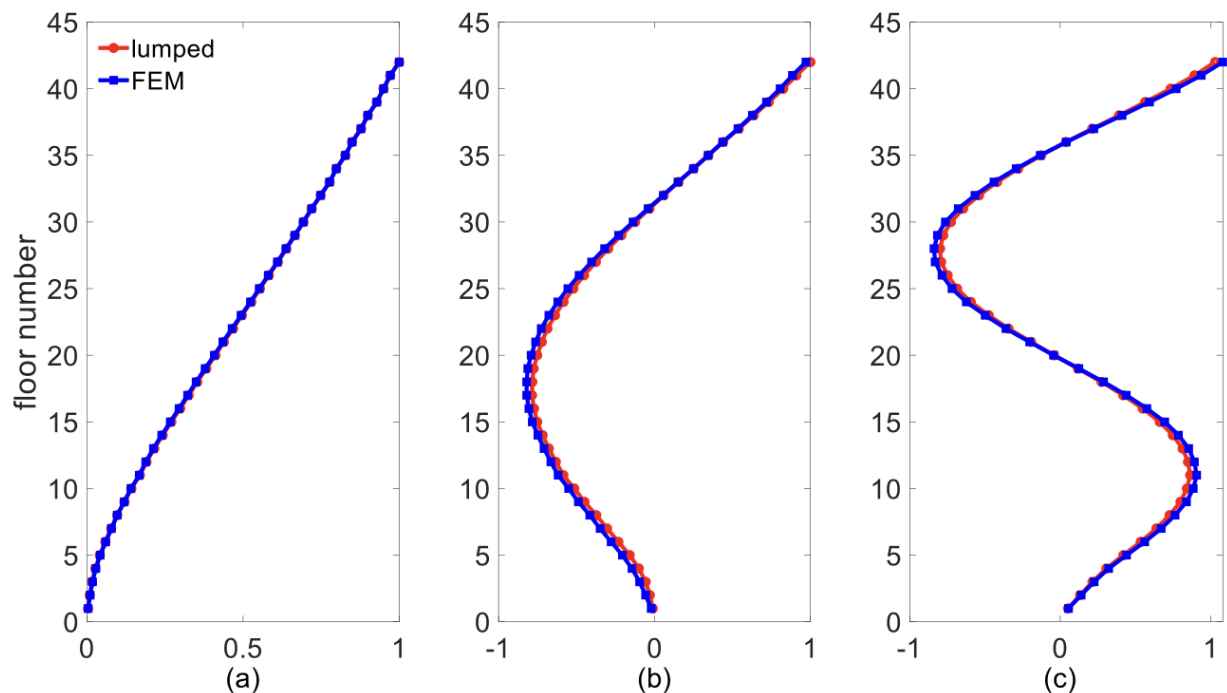


Figure 4. Mode shape comparison between FEM and lumped mass model in x-direction: (a) first mode, (b) second mode, and (c) third mode.

Table 2. Comparison of natural frequencies of FEM and lumped mass model.

Modes	Lumped Mass Model	3D FEM
1	0.389 Hz	0.389 Hz
2	1.466 Hz	1.465 Hz
3	1.984 Hz	1.991 Hz

4. Tuned Mass Damper Inerter (TMDI) and the Equivalent TMD

4.1. Structural Control

The notion of vibration control in civil engineering was presented more than a century ago in Japan. During World War II, many concepts of vibration isolation, absorption, and damping were developed [39]. Recently, significant attention has been paid to the design and development of vibration control devices with a significant emphasis on improving wind and earthquake responses in buildings. In the last two decades, the focus has been on developing control strategies built with workable technology that can be implemented at full scale [40]. Supplemental energy dissipation strategies using passive, active, hybrid, and semi-active devices offer inviting ways to protect buildings and bridges from seismic and wind actions [41,42]. Passive vibration absorbers such as tuned mass dampers (TMD) and viscous dampers (VD) are primarily recognized and widely approved by the civil engineering community as a way of suppressing the impacts of dynamic loads [43–47].

Tuned vibration absorbers work efficiently in reducing vibrations in slender structures under resonance [48]. Due to the inability of passive devices to adjust to changes in structural parameters and external loadings, active and semi-active devices have become popular because they are relatively robust and smaller in size [49,50]. A non-conventional TMD characterized by a high mass ratio was realized via inter-story isolation [51]. A TMD was optimized for minimizing the dynamic responses of a cantilever beam [52]. Full-scale implementation of active dampers can be observed mainly in Japan, the United States, and China. However, due to high power consumption, increased capital and maintenance costs, and reduced reliability and stability issues of an active control system, construction industries do not recommend this control system. Semi-active control looks promising because it can reduce/eliminate the limitations of passive and active control while taking advantage of both control systems [53]. Semi-active control can maintain the same performance level, adaptability, and versatility as active control without requiring an ample power supply. Design strategies, control performance of devices, and their applications in the real world can be found in Refs. [39,40,54–56]. An integrated passive damping system has been introduced lately to mitigate vibration in tall buildings where a portion of the structural mass is used as TMD [57]. Modified tuned liquid dampers with soil-structure interaction have also been studied for seismic protection of buildings [58]. A new study has shown that an energy-harvesting damper could be implemented in smart structures using cutting-edge technologies [59].

4.2. Tuned Mass Damper Inerter (TMDI)

Over the past few decades, TMD has been used widely in tall buildings and long-span bridges as a supplemental damping device to mitigate the vibration induced by wind loads to meet the serviceability criteria prescribed by the standard codes [60]. TMD, in its simplest form, is a mass connected to the main structure via linear spring (stiffness) and damping elements (dampers) [61]. Lately, Marian and Giaralis [62] have proposed a new device called TMDI by incorporating an inerter in classical TMD, as shown in Figure 5.

By definition, the force developed in the ideal linear inerter is given as:

$$f = b(\ddot{u}_1 - \ddot{u}_2) \quad (3)$$

where \ddot{u}_1 and \ddot{u}_2 are the acceleration across two terminals, and b is the constant called inertance, which has the mass unit. In this study, a rack and pinion flywheel-based inerter is considered, as shown in Figure 5. The inertance of the device can be described as [63,64]:

$$b = m_f \frac{\gamma_f^2}{\gamma_{pf}^2} \left(\prod_{q=1}^n \frac{r_q^2}{pr_q^2} \right) \quad (4)$$

where m_f is the mass of the flywheel, γ_{pf} is the radius of gyration, and $\frac{r_q}{pr_q}$ is the gear ratio. It can be seen from equation (4) that the inertance of the device can be increased significantly by increasing the gearing ratio and the number of gears. Thus, the inertance can be scaled up without increasing the device's mass, which is analogous to a viscous damper where the viscous damping coefficient can be increased significantly without a considerable increase in the mass of the damper. However, many experimental studies have suggested that the physical mass of an inerter device with a large apparent mass cannot be ignored [65,66]. A hydraulic inerter damper has been introduced recently to produce a significantly large inertance with a smaller physical mass of the device [67]. The inerter has been implemented successfully in auto industries and for developing suspension in the train [68]. Recently, this device has been studied for its application in civil engineering structures. The optimal design of passive TMDI for vibration control of support-excited structural systems has been studied. The optimal parameter of TMDI for minimizing displacement variance of the primary structure has been obtained analytically [62,69].

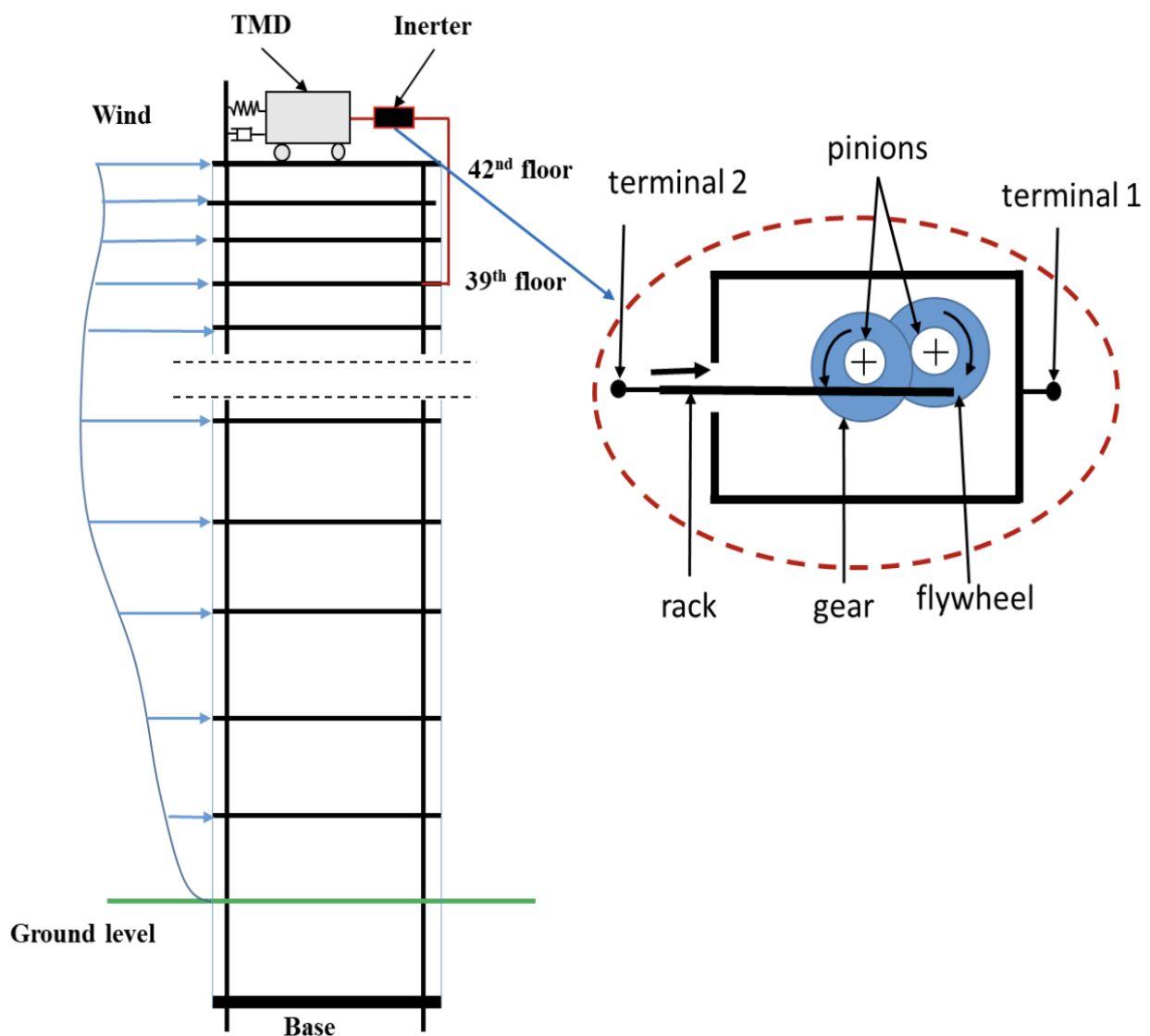


Figure 5. Schematic of a high-rise building equipped with a TMDI.

4.3. Equivalent TMD

Three significant assumptions exist in the literature about using the tuned mass damper inerter (TMDI) for vibration control. First, most of the literature has ignored the physical mass of the inerter device. Second, most earlier studies have assumed the ideal inerter with 100% efficiency. Third, the inerter is considered a linear device with constant inertance. However, building an inerter with zero mass and 100% efficiency in a real-world application is prohibitive. Furthermore, an experimental investigation has shown that the inerter cannot behave linearly, especially at low frequencies, due to the dominance of friction [65]. Finally, none of those assumptions are fully valid from the engineering design perspective, which means that the TMDI might perform differently when designed in real-world applications compared to what has been reported in the literature.

When inerters are used for high-rise buildings, a high value of inertance (apparent mass) is expected (in the range of tons). To produce such inertance, an inerter with a significantly sizeable physical mass is needed. Because most of the earlier research has been focused on analytical studies and numerical simulations, there have been few experimental investigations to comprehend the properties of the inerter device and its performance. Based on the experiment performed at Cambridge University, an inerter with a 3.5 kg physical mass can produce an inertance of approximately 700 kg [65]. Another similar study suggested that the

inertor with a bodily mass of 1 kg could create an inertance of 180 kg [66]. An experimental study at Oklahoma State University showed that 180 kg inertance was produced by the rack and pinion inertor with a physical mass of 2 kg, giving a specific inertance of approximately 90 [70]. The study shows that the specific inertance (inertance per unit physical mass) can vary from 90 to 200. In the best-case scenario, the particular inertance of 200 can be considered to calculate the physical mass [71]. For a fair comparison of control performances, the physical mass of the inertor is added to the mass attached to get the equivalent mass of TMD, as expressed by Equation (5).

$$m_{eq} = m + \left(\frac{b}{200}\right); \quad \mu_{TMD} = \mu_{TMDI} + \left(\frac{\beta}{200}\right); \quad \beta = \frac{b}{M} \tag{5}$$

where m_{eq} is the mass of equivalent TMD, m is the attached mass, b is the inertance of the inertor in kg, and M is the first modal mass of the building. It has been reported that the optimal performance of TMDI is observed when the inertance ratio ranges between 0.3 to 0.6, in consideration of practical applications [71,72]. This paper considers an inertance ratio of 0.5 to compare the performance with an equivalent linear tuned mass damper (TMD). Both equivalent TMD and TMDI are optimized under filtered white noise excitations for one-to-one comparison.

5. Structural Modeling with TMDI

The lumped mass system of the 42-story building developed in Section 3 is considered in this section to derive the equation of motion with the TMDI. However, to generalize the dynamic equations, a 42-story building with 42 degrees of freedom equipped with TMDI at any location defined by the location vector is considered. The proposed TMDI consists of TMD with mass m at the top of the building, and the mass of TMD is attached to the building through a linear spring of stiffness k and linear dashpot with damping coefficient c . One terminal of the inertor is connected to the mass of TMD. The other terminal can be connected to any lower floor of the building so that there is a difference in acceleration between the two points, which determines the control force based on equation (3). For this study, the first terminal is connected to TMD. Another terminal is connected to the third floor from the top (39th story), as shown in Figure 5. Consider $X_s \in \mathbb{R}^{42}$ be the relative floor displacement vector, $L_b \in \mathbb{R}^{42}$ the location vector that specifies the floor where another terminal is connected (the first terminal is connected to TMD), and $L_d \in \mathbb{R}^{42}$ the location vector for the damper in the building. It should be noted that all the elements of L_d are zero except a single one at a particular location where the TMD is located.

Similarly, all the elements of L_b are zero except a single one. By doing this, it is possible to define a vector $L_c = L_d - L_b$, which specifies the location of both terminals of the inertor. L_c contains zero elements, except 1 at the first terminal (where TMD is connected) and -1 at the second terminal (where the floor is attached). $M_s \in \mathbb{R}^{42 \times 42}$, $C_s \in \mathbb{R}^{42 \times 42}$, and $K_s \in \mathbb{R}^{42 \times 42}$ are the mass, damping, and stiffness matrices of the lumped mass system building developed in the previous section. Now, the coupled equation of motion of the building and TMDI under the wind load can be written as:

$$\left. \begin{aligned} (M_s + L_d m L_d^T + L_c b L_c^T) \ddot{X}_s + (m L_d + b L_c) \ddot{y} + C_s \dot{X}_s + K_s X_s &= F \\ (m + b) \ddot{y} + (m L_d^T + b L_c^T) \dot{X}_s + c \dot{y} + k y &= 0 \end{aligned} \right\} \tag{6}$$

where $F \in \mathbb{R}^{42}$ is the vector of wind loads acting on each floor. In general, wind load acting on the mass of TMD is not included in the equation because it is usually located inside the building with no exposure to wind load, or the wind load acting on the TMD mass is negligible. However, the earthquake-induced inertial load cannot be ignored under

the seismic event. Thus, the equation of motion of structure equipped with TMDI under seismic excitation can be described as:

$$\left. \begin{aligned} (\mathbf{M}_s + \mathbf{L}_d m \mathbf{L}_d^T + \mathbf{L}_c b \mathbf{L}_c^T) \ddot{\mathbf{X}}_s + (m \mathbf{L}_d + b \mathbf{L}_c) \ddot{y} + \mathbf{C}_s \dot{\mathbf{X}}_s + \mathbf{K}_s \mathbf{X}_s &= -\mathbf{M}_s \Lambda \ddot{x}_g \\ (m + b) \ddot{y} + (m \mathbf{L}_d^T + b \mathbf{L}_c^T) \dot{\mathbf{X}}_s + c \dot{y} + ky &= -m \ddot{x}_g \end{aligned} \right\} \quad (7)$$

where Λ and \ddot{x}_g are the floor location vector and ground acceleration, respectively.

From Equation (7), the following terms can be defined

$$v = \frac{\sqrt{\frac{k}{(m+b)}}}{\omega_1}; \quad \zeta = \frac{c}{2\sqrt{(m+b)k}}; \quad \beta = \frac{b}{M}; \quad \mu = \frac{m}{M} \quad (8)$$

where ω_1 is the natural frequency of the building for the first mode, and M is the modal mass of the building. v , ζ , β , and μ are the frequency ratio, the damping ratio of TMDI, the inertance ratio, and the mass ratio, respectively. It is crucial to note that if $b = 0$ in the above equations, TMDI converts into TMD.

Advanced numerical methods are applied in MATLAB to solve the dynamic equations [73]. The timber-hybrid building equipped with the TMD, TMDI, and pendulum PTMD is modeled in state space [74]. The trial-and-error method finds the proper solver and convergence. Initially, automatic solver selection with a variable time step was assigned but could not solve the equations. In the second step, an ode45 (Dormand–Prince) solver with an absolute tolerance of 1×10^{-6} was used. It solved the equations under the harmonic excitation and the variable frequency excitations but failed under earthquake excitations. In the third step, the ode4 (Runge–Kutta) solver was used with a fixed time step of 0.01 s, which produced good results before the impact between the pounding mass and the boundary but failed later. Finally, an ode4 (Runge–Kutta) solver with a fixed time step of 1×10^{-3} s was able to capture the dynamics of impact. It was observed that the time step influenced simulation results.

Excitation Forces

To reflect the wind and seismic loads that the structure may experience during its lifetime, white-noise excitations and variable frequency (VF) sinusoidal excitations are applied to the building. Both excitations are different in energy and frequency content, as shown in Figure 6. Gaussian white noises are passed through a bandpass filter to match the excitations with wind loads acting on tall buildings [75]. It should be noted that the white noise excitation has higher energy at lower frequencies, and energy decreases as the frequency increases, as shown in Figure 6. This energy distribution pattern over frequency is observed in wind tunnel experiments of high-rise buildings [55]. Usually, tall buildings are exposed to wind and seismic loads that contain broadband frequency. To represent the excitations with broadband frequency, sinusoidal excitation with a linear frequency variation is applied to the building. In this case, the excitation frequency is increased from 0.05 Hz to 4 Hz at an interval of 0.0263 Hz. The power spectrum of the VF excitation shows high energy over a wide frequency range (0.05 Hz to 1.4 Hz). The energy decreases sharply when the frequency increases. The optimal parameters of both TMD and TMDI are obtained under filtered white noise and VF excitations.

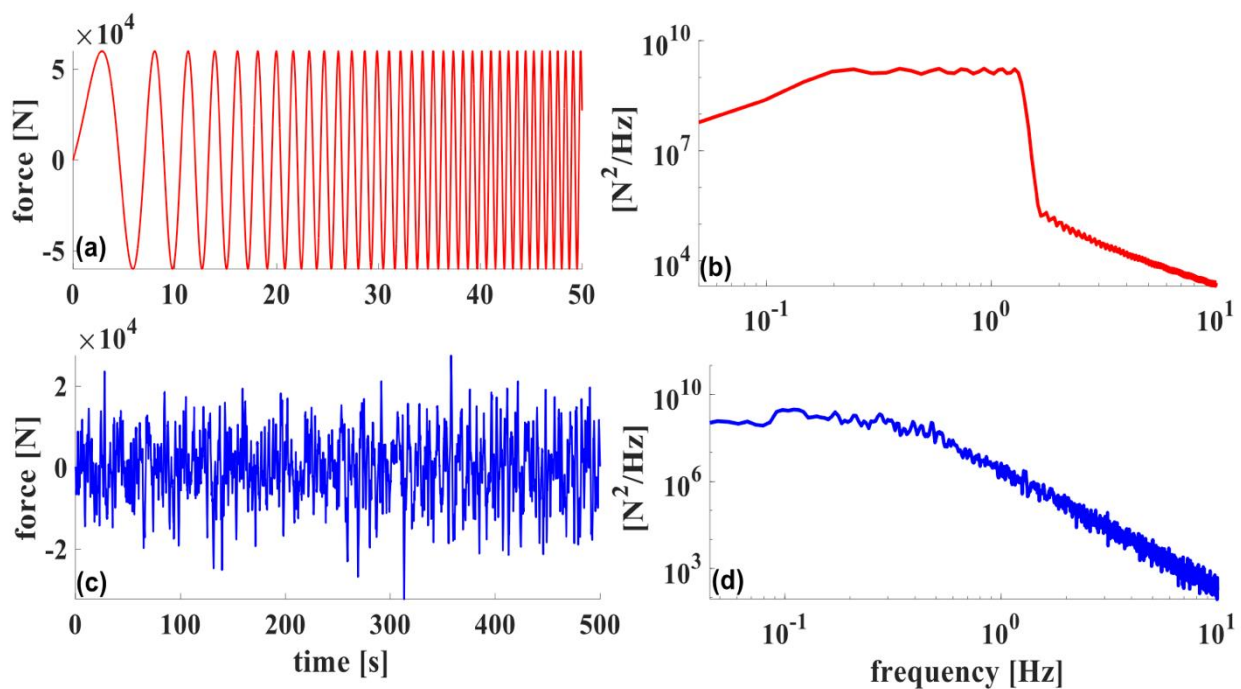


Figure 6. Excitation forces: (a) time history of a variable frequency sine wave, (b) spectrum of the VF sine wave, (c) time history of filtered white noise, and (d) the corresponding spectrum of the filtered white noise excitation.

6. Optimization of TMDI and Equivalent TMD

Finding the optimum device parameters to reduce excessive vibration is crucial. In this section, the TMD and the TMDI are optimized under the filtered white-noise excitations and VF excitation discussed in the previous section. The TMDI is optimized for different mass ratios starting from 0.5% to 5%, whereas the inertance ratio is chosen to be 0.5 because it is much more realistic based on previous studies. The equivalent linear TMD results in a 0.25% increase in mass ratio compared to TMDI by considering the physical mass of the inerter corresponding to the inertance ratio of 0.5. Thus, the resulting mass ratio of TMD ranges from 0.75% to 5.25%. A wide range of damping and frequency ratios can be considered for the given mass ratio to find the optimal device properties. The frequency ratio varies between 0.7 and 1.4, while the damping ratio changes between 0.1% and 20% under filtered white noise excitations. The choice of the device's best parameters relies on the optimization objectives. The optimum device properties for the reduction of displacement response of the structure may not be optimal for the decrease in acceleration response and vice versa.

Figure 7a,b shows the variation of the normalized acceleration of the 42nd floor with frequency and damping ratios of TMDI and equivalent TMD, respectively. It is observed that for a 1% mass ratio, the optimum frequency ratio for the TMDI is higher (1.042) compared to the optimum frequency ratio for TMD (1.004). However, the optimum damping ratio for both devices remains almost the same, as shown in Figure 7. TMD reduces the acceleration by 54.54%, and TMDI reduces the same response by 51.58%. Figure 8 shows the optimal device properties considering the 5% mass ratio for minimizing normalized acceleration at the top floor. TMD and TMDI perform better when the mass ratio increases from 1% to 5%. However, these devices' optimum frequency and damping ratios are far from close. For the 5% mass ratio, the optimum frequency ratio for TMDI is 1.011, but the optimum frequency ratio for TMD is 0.949.

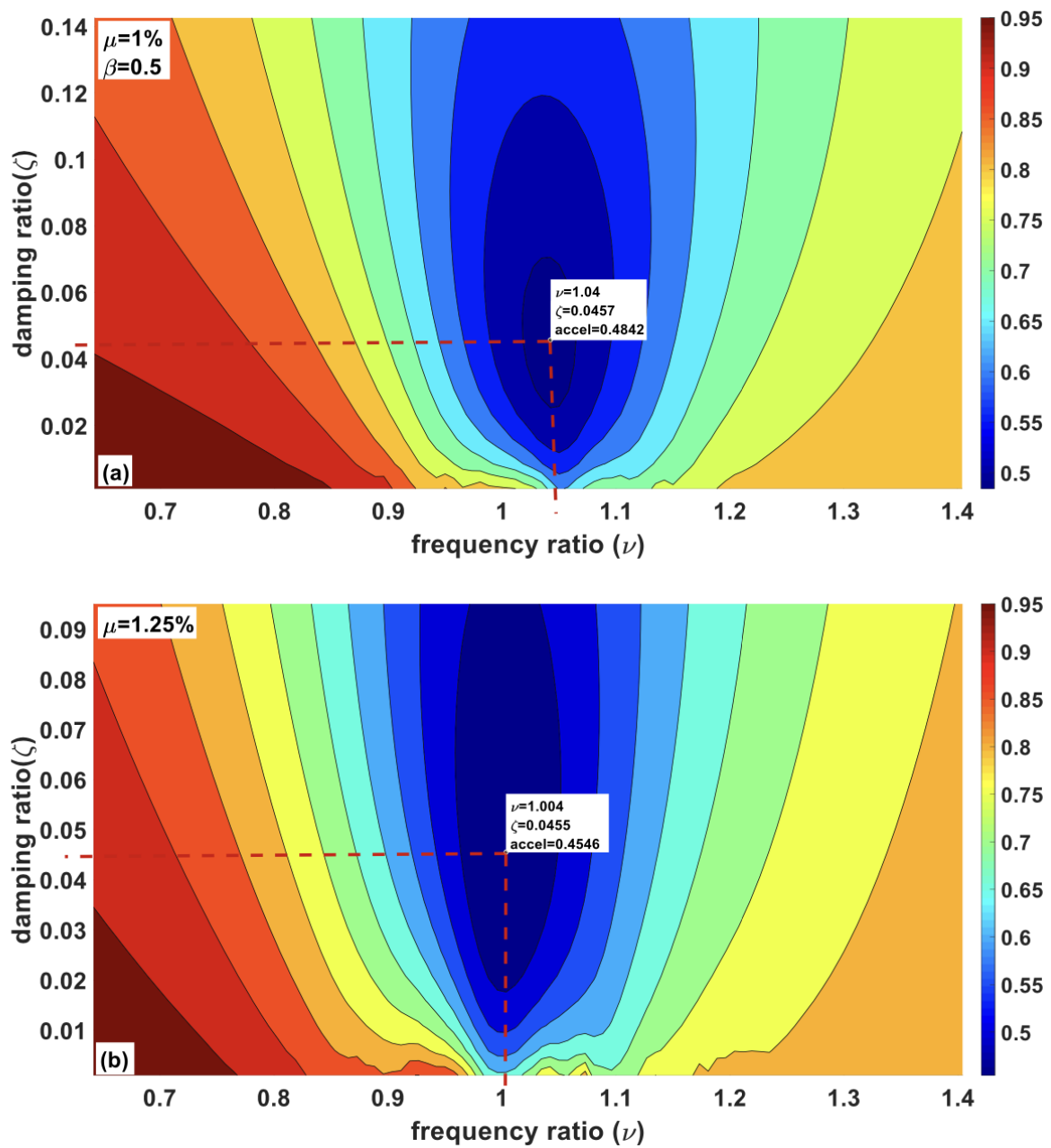


Figure 7. Optimization of the TMDI (the mass ratio is 1% and the inertance ratio is 0.5) and the equivalent TMD under filtered white noise excitations: (a) minimizing acceleration at the top floor using TMDI and (b) minimizing acceleration at the top floor using equivalent TMD.

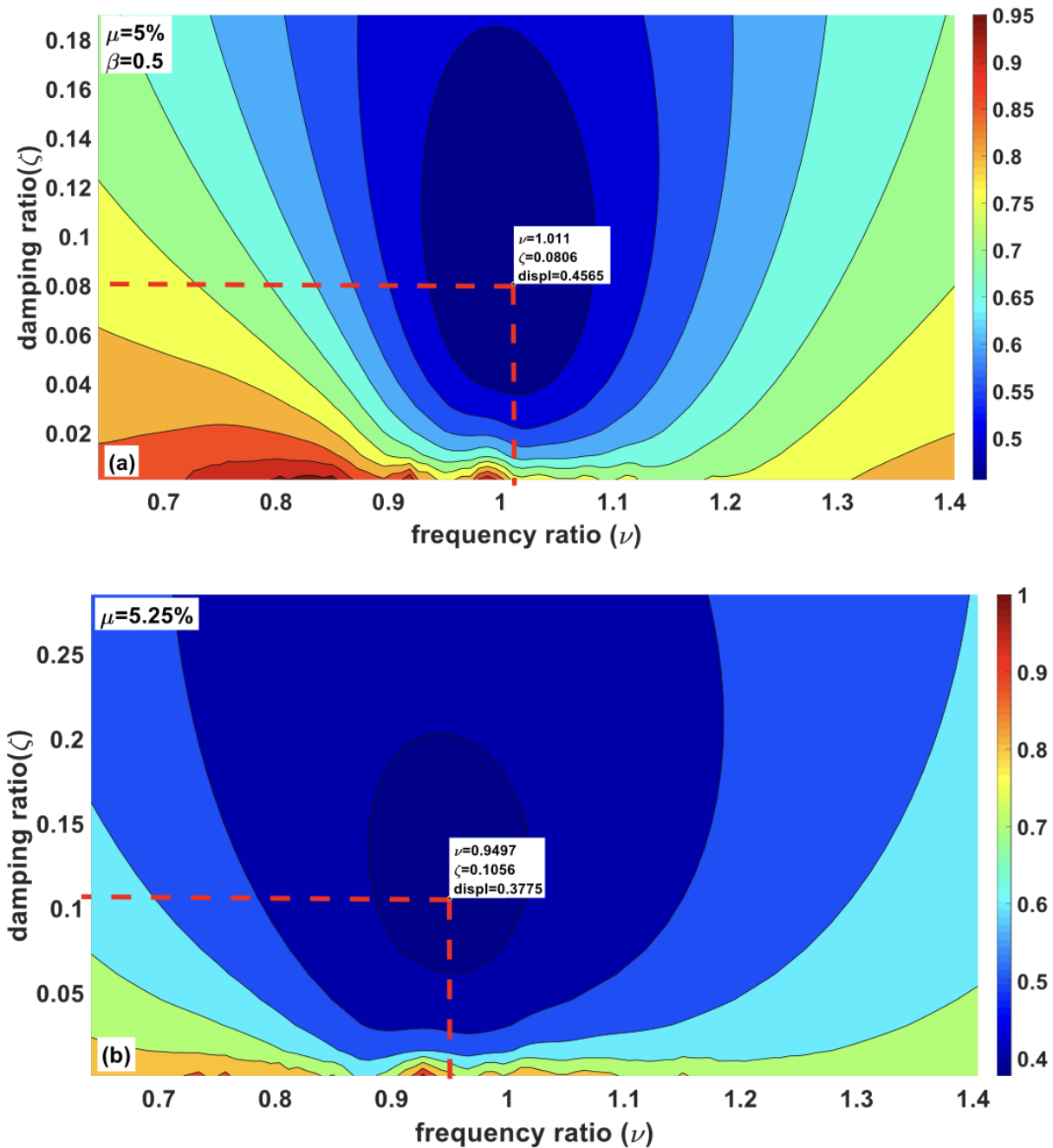


Figure 8. Optimization of TMDI (the mass ratio is 5% and the inertance ratio is 0.5) and equivalent TMD under filtered white noise excitation: (a) minimizing displacement at the top floor using TMDI, and (b) minimizing displacement at the top floor using equivalent TMD.

Similarly, the optimal damping ratio for TMDI is 8.06%, and the optimal damping ratio for TMD is 10.56%. When the mass ratio increases, optimal parameters for TMD and TMDI move far from each other, which can be well described by comparing Figures 7 and 8. In many previous studies, optimal properties for TMDI are used for TMD without considering the physical mass of the inerter device. This shortage undermines the capability of linear TMD in two ways: the mass ratio of equivalent TMD becomes small, which results in reduced performance; conversely, by connecting the inerter with TMD, the optimum damping ratio and frequency ratio of the TMD are lost, which leads to lower performance. For example, TMDI with a 5% mass ratio reduces top floor acceleration by 58.8% and

displacement by 54.35%, while the same responses are reduced by 65.78% and 62.25% using equivalent TMD.

For both TMDI and TMD, the optimum damping ratio increases, and the optimum frequency decreases as the mass ratio increases. However, the optimum frequency ratio remains above 1(1.019) for TMDI to minimize acceleration when the mass ratio increases up to 5%. Still, the optimum frequency ratio for equivalent TMD decreases relatively fast and falls below 1(0.980). Therefore, as shown in Table 3, optimal parameters are different for the same device depending upon the minimization objectives. For example, the highest reduction in acceleration at the top floor is achieved when the damping ratio is 12.06%, and the frequency ratio is 0.98. Still, the maximum decrease in displacement is achieved when the damping ratio is 10.56% and the frequency ratio is 0.949 for the equivalent TMD with a mass ratio of 5%. In contrast, TMDI has the same optimal damping ratio for reducing displacement and acceleration responses, even though the optimal frequency ratios are different.

Table 3. Optimal parameters of the TMDI and the equivalent TMD, under variable frequency excitation, for different mass ratios.

TMD Parameters			% Age Reduction		TMDI Parameters			% Age Reduction		
μ (%)	v_{opt}	ζ_{opt}	Accel.	Displ.	μ (%)	Beta	v_{opt}	ζ_{opt}	Accel.	Displ.
0.75	1.004	0.044	34.46	–	0.5	0.5	1.034	0.046	36.05	–
	0.996	0.044	–	39.7			1.027	0.046	–	40.06
1.25	1.004	0.053	39.11	–	1	0.5	1.034	0.053	37.56	–
	0.988	0.053	–	45.21			1.027	0.053	–	41.36
2.25	0.995	0.070	44.20	–	2	0.5	1.027	0.060	40.21	–
	0.988	0.070	–	51.32			1.019	0.053	–	44.30
3.25	0.995	0.090	47.32	–	3	0.5	1.027	0.066	42.41	–
	0.980	0.090	–	54.94			1.011	0.066	–	46.66
4.25	0.995	0.110	49.53	–	4	0.5	1.019	0.073	44.45	–
	0.972	0.100	–	57.46			1.011	0.066	–	48.68
5.25	0.9959	0.1001	51.05	–	5	0.5	1.019	0.0867	46.19	–
	0.9651	0.1101	–	59.37			1.004	0.8006	–	50.46

Table 4 shows that as the mass ratio of both devices increases, the difference between the control performance of TMD vs. TMDI increases. For example, at a 1% mass ratio equivalent, TMD reduces top floor acceleration by an extra 1.55% and displacement by an additional 3.85% compared to TMDI. Still, at a 5% mass ratio, the same responses are reduced by an extra 4.86% and 8.91%, respectively.

Table 4. Optimal parameters of TMDI and equivalent TMD for the different mass ratios.

TMD Parameters			% Age Reduction		TMDI Parameters			% Age Reduction		
μ (%)	v_{opt}	ζ_{opt}	Accel.	Displ.	μ (%)	Beta	v_{opt}	ζ_{opt}	Accel.	Displ.
0.75	1.006	0.036	49.80	–	0.5	0.5	1.047	0.040	50.09	–
	1.006	0.036	–	47.7			1.037	0.040	–	47.60
1.25	1.004	0.046	54.54	–	1	0.5	1.042	0.045	51.58	–
	0.995	0.046	–	52.21			1.034	0.045	–	48.81
2.25	1.002	0.068	59.16	–	2	0.5	1.042	0.053	53.94	–
	0.998	0.068	–	56.32			1.027	0.053	–	50.66
3.25	0.995	0.075	61.97	–	3	0.5	1.034	0.060	55.90	–
	0.972	0.088	–	58.84			1.027	0.060	–	52.10
4.25	0.988	0.105	64.08	–	4	0.5	1.027	0.063	57.75	–
	0.957	0.105	–	60.76			1.019	0.063	–	53.19
5.25	0.980	0.120	65.78	–	5	0.5	1.019	0.080	58.83	–
	0.949	0.105	–	62.25			1.011	0.080	–	54.35

6.1. Effect of Mass Ratio and Inertance Ratios on the Performance of TMDI

Control performance of the TMDI with the inerter connected between TMD at the top and 39th floor is investigated against varying mass ratio and inertance ratio under filtered white-noise excitations. Four unitless parameters are defined based on the controlled and uncontrolled responses as follows:

$$\left. \begin{aligned} R_1 &= \frac{\text{STD displacement at top floor (controlled)}}{\text{STD displacement at top floor (uncontrolled)}} \\ R_2 &= \frac{\text{STD acceleration at top floor (controlled)}}{\text{STD acceleration at top floor (uncontrolled)}} \\ R_3 &= \frac{\text{Peak displacement at top floor (controlled)}}{\text{Peak displacement at top floor (uncontrolled)}} \\ R_4 &= \frac{\text{Peak acceleration at top floor (controlled)}}{\text{Peak acceleration at top floor (uncontrolled)}} \end{aligned} \right\} \quad (9)$$

As defined by Equation (9), R_1 and R_2 represent the performance of TMDI for the reduction of root mean square (RMS) displacement and acceleration at the top floor, whereas R_3 and R_4 represent the performance for the reduction of peak displacement and peak acceleration at the top floor. Figure 9 shows the three-dimensional (3D) plot of normalized structural responses with respect to mass and inertance ratios. The normalized 3D plot of standard deviation (STD) and peak responses are then projected into the μ - β plane, as shown in Figure 9.

Figure 9a shows the variation of STD displacement, and Figure 9b shows the variation of STD acceleration. Figure 9c shows the variation of peak displacement. Figure 9d shows the variation of peak acceleration of the top floor with respect to μ and β . All the controlled responses are normalized by dividing their corresponding uncontrolled responses as defined by Equation (9). It is crucial to notice that the first line along the μ axis is the performance of pure TMD because there is a negligible inertance ratio.

Similarly, the first line along the β axis is the pure tuned inerter damper (TID) with no mass attached at the top. Except for the first two lines along each axis, the device acts as TMDI. As discussed in the previous sections, for the sizeable inertance value, the physical mass of the device could be significantly high. For a given mass ratio, a small inertance ratio reduces the device's performance because it damages the optimum frequency and damping ratio, resulting in less energy dissipation. It is observed in Figure 9a,b that there is no significant reduction in the responses when the β increases beyond 0.6.

Similarly, peak displacement and acceleration may remain constant when β is increased beyond 0.5, as shown in Figure 9c,d. The optimum β for a given mass ratio cannot be too small (close to zero) or too large (close to 1). This observation is supported by several analytical and experimental studies on TMDI, as described in the previous sections. An enlarged view of Figure 9a, which illustrates the effect of mass ratio and inertance ratio on the STD displacement of the top floor, is shown in Figure 10.

In Figure 10, point A represents the virtually uncontrolled case where the mass ratio is 1×10^{-5} , and the inertance ratio is 1×10^{-10} . Thus, the value of R_1 is equal to 1 at point A. The curve that goes through points A, B, and C is the typical TMD with a frequency ratio of 0.99 and a damping ratio of 8.5%. Those parameters (frequency ratio of 0.99 and damping ratio of 8.5%) correspond to a 3% mass ratio. Unless otherwise mentioned, this value (3% mass ratio) has been used entirely in the paper. At points B and C, the mass ratio is nearly 2% and 4%, respectively, but the inertance ratio remains negligible (1×10^{-10}). The response reduction is sharp from point A to B but flatter from point B to C. With the mass ratio increase from 0 to 2%, STD displacement is reduced by nearly 55%. However, when the mass ratio increases by 2% (2% to 4%), the extra reduction in the response is only 4%. This observation suggests that a significant impact on the mass ratio can be observed when the mass of TMD is smaller. A curve through points A, D, and E represents the typical tuned inerter damper (TID), where the attached mass is almost zero.

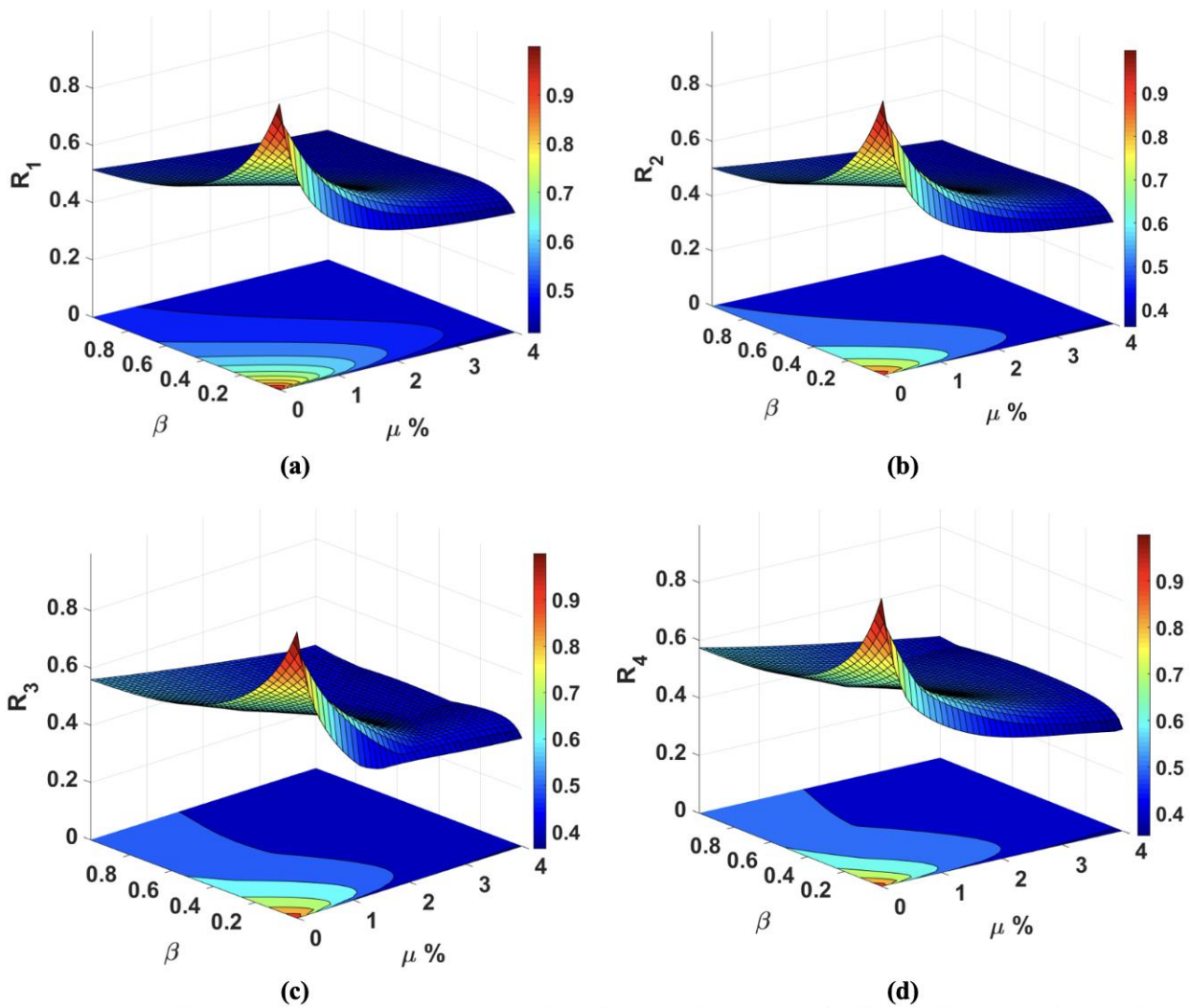


Figure 9. Effect of the inertia ratio and the mass ratio on the structural responses under filtered white-noise excitations: (a) RMS displacement at the top floor, (b) RMS acceleration at the top floor, (c) peak displacement at the top floor, and (d) peak acceleration at the top floor.

From point A to D, the STD displacement at the top floor decreases sharply, and the reduction rate decreases as we go from point D to E. This pattern in TID is similar to that observed in TMD, where the inertia ratio of TID is analogous to the mass ratio of TMD. If we consider any point between points A and C and move along β axis, the response increases for smaller values of the inertia ratio. Here, the inerter negatively impacts the energy-dissipating capacity of the TMD. As defined by Equation (5), the inertia ratio increases the mass of equivalent TMD. Even if the equivalent mass is not considered, STD displacement reduced by TMD at a 4% mass ratio is more significant than TMDI with the same mass ratio and an inertia ratio of 0.9. Thus, the curve representing linear TMD (curve through points A, B, and C) performs better than any other parallel lines. This finding strengthens the argument that linear TMD with optimum parameters can serve better than TMDI.

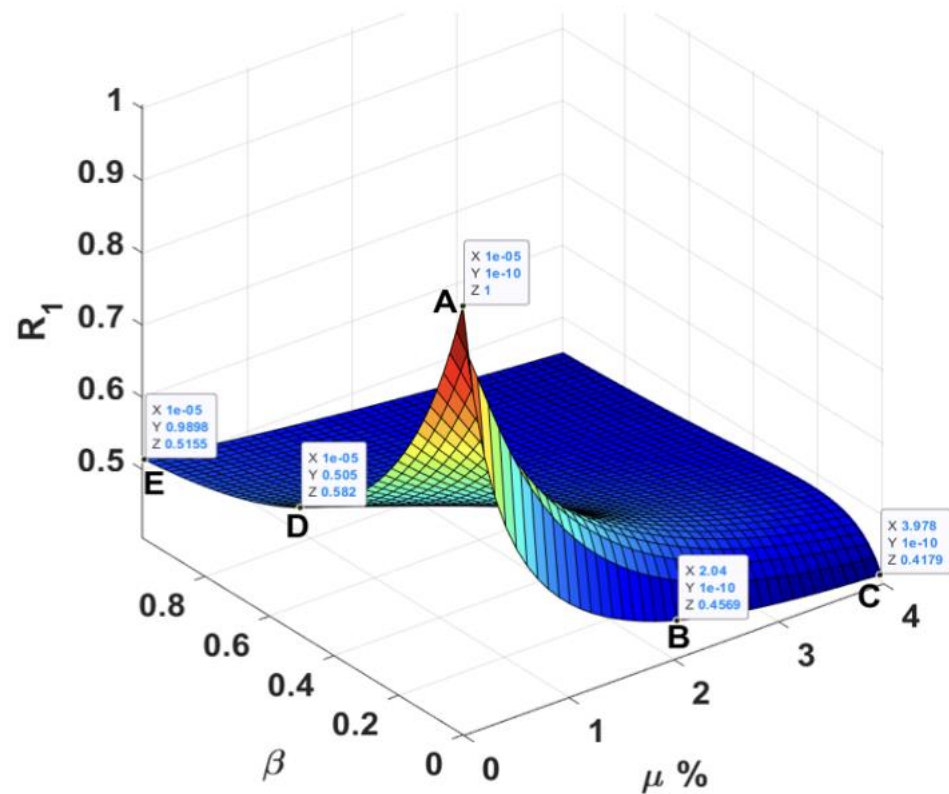


Figure 10. Effect of inertia and mass ratios on the acceleration response under filtered white noise excitations.

6.2. Performance under Variable Frequency Sinusoidal Excitations

The performance of both TMD and TMDI is compared at various mass ratio scenarios using VF sinusoidal excitations. The optimal device properties are obtained by running simulations in MATLAB for a wide range of frequency and damping ratios under VF excitations (0.05 to 4 Hz).

Figure 11a shows the optimization of TMD parameters, and Figure 11b shows the optimization of TMDI parameters under variable frequency sinusoidal excitation. The optimum parameters of both devices for various mass ratios are listed in Table 3. Figure 11 shows both devices' most favorable frequency and damping ratios. It is observed that those parameters are different for each device to minimize the acceleration of the building. Similar to white noise excitations, under VF excitations for a 2% mass ratio, the optimal frequency ratio for TMD is smaller than 1 (0.988). It is greater than 1 (1.019) for TMDI. However, the optimal damping ratio is slightly higher in the case of TMD compared to TMDI. The performance of both devices increases as the mass ratio increases, as listed in Table 3. In both devices, the optimal frequency and damping ratio decrease as the mass ratio increases. Figure 12 shows the time history of displacement and acceleration of the top floor under VF excitations, and Figure 13 shows their corresponding response spectra. Optimized equivalent TMD reduced the STD displacement by 50%, whereas optimized TMDI reduced the same responses by only 43%. Similarly, peak displacement at the top floor is reduced by 17.9% using TMD, but TMDI reduces the peak displacement by 9.8%. This finding shows that optimized equivalent TMD has better control performance than TMDI when the physical mass of the inerter is considered.

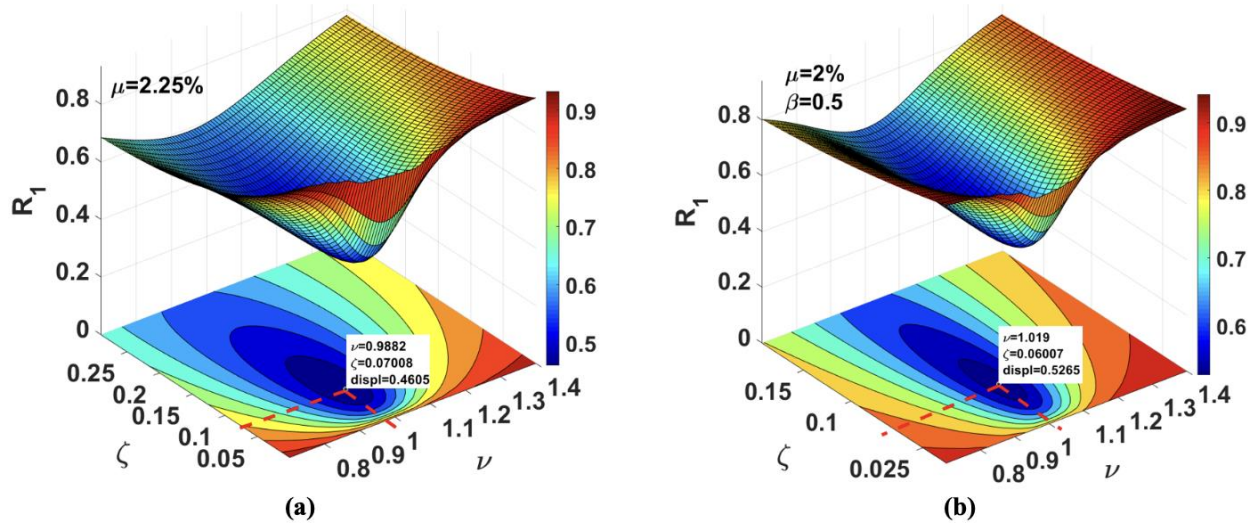


Figure 11. Optimization for minimizing RMS displacement at the top floor, under variable frequency excitation: (a) TMD and (b) TMDI.

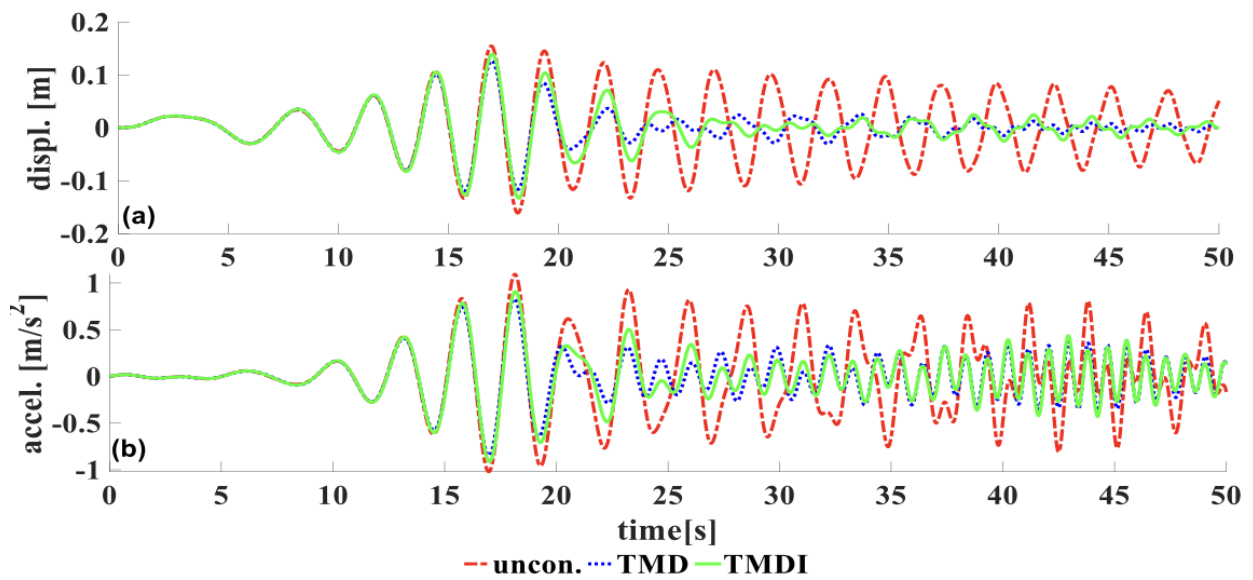


Figure 12. The response of the 42nd floor under VF sinewave loadings: (a) displacement time history and (b) acceleration time history.

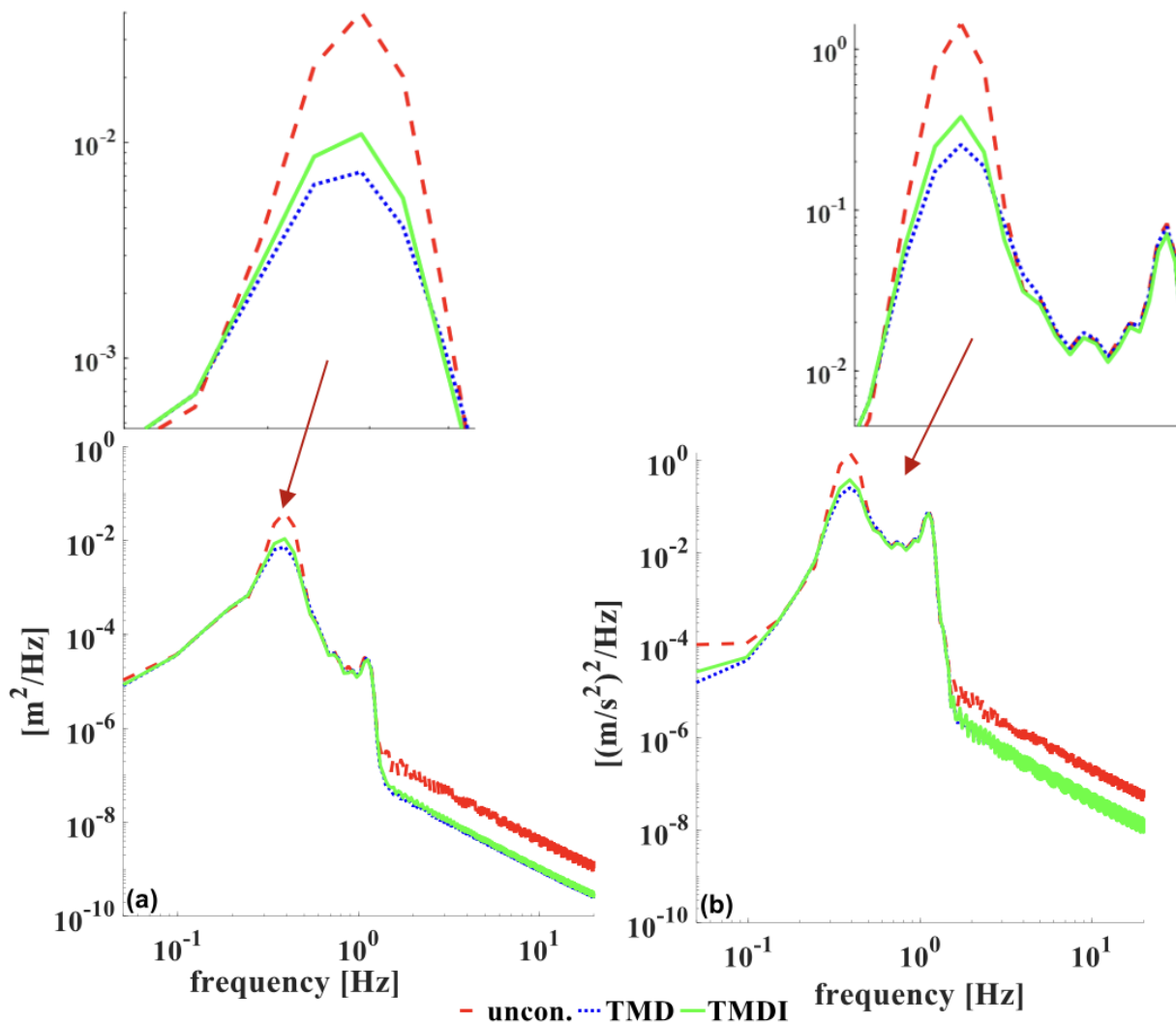


Figure 13. Responses of the 42nd story under variable frequency excitation: (a) displacement and (b) acceleration spectra.

7. Pounding Tuned Mass Damper

Similar to the nonlinear dynamic behavior of base-isolated buildings with friction pendulum systems under earthquakes [76], the core idea of the pounding tuned mass dampers is to produce nonlinear behavior under external excitations, with better performance in reducing a broad band of excitation frequencies. A pounding tuned mass damper (PTMD) is a modified TMD where the motion of the TMD is strained by using viscoelastic material at the boundary. PTMD has two distinct phases in its working principle. In phase one, the excitation energy is absorbed by the PTMD mass from the primary structure. In phase two, the absorbed energy is dissipated when the restrained mass collides with the viscoelastic boundary. A PTMD was introduced to attenuate the excessive vibration in transmission towers under an earthquake, where the peak displacement was reduced by 41% and the peak acceleration was reduced by 34% [77]. The performance of PTMD was investigated using numerical and experimental methods to reduce the vibrations in pipes. The PTMD was built by integrating TMD with an impact damper. The result showed that PTMD reduced the vibrations significantly in horizontal and vertical directions, which could improve the fatigue life of the structure [78,79]. An L-shaped pounding device designed for the vibration attention of a jumper was set up in the middle of the jumper to investigate its performance. The result showed that PTMD performs better than regular TMD under free and forced vibrations [80,81]. Optimized multiple-tuned mass dampers are shown to be effective

devices and demonstrate exemplary performance in reducing the vibration of bridges due to moving vehicles [82]. A numerical simulation of multiple PTMD was performed to suppress the vibration induced by wind and traffic load on the bridges. The simulation results showed that both single and multiple PTMDs effectively reduce the vibration caused by the combination of wind load and traffic load on the bridge. PTMD can suppress the vibration induced in the bridge due to moving vehicles [83]. PTMD based on pendulum TMD has been studied for the vibration suppression of a single-degree-of-freedom system [84].

7.1. Proposed Pendulum PTMD

Chapain and Aly [85] proposed a pounding device called “pendulum PTMD” by modifying the pendulum TMD to control the vibration in wind turbines where the pounding happens on one side of the boundary. Extensive numerical simulation has been performed to obtain the optimal frequency ratio and pounding stiffness to attenuate the excessive vibration induced by wind and earthquake loads. It has been observed that pendulum PTMD has enhanced performance compared to traditional TMD to reduce both acceleration and displacement of wind turbines under seismic excitations. It was realized that the optimal tuning ratio for pendulum PTMD is distant from classical TMD. The optimal device properties are obtained from a previous study and implemented in a 42-story timber building. This study considers the distance between the pounding mass and the boundary zero, a pounding stiffness of $\alpha = 2.19 \times 10^6 \text{ Nm}^{-1.5}$, and an optimal frequency ratio of 0.78, based on the charts designed by Chapain and Aly [85].

7.2. Modeling of a Building Equipped with Pendulum PTMD

A pendulum PTMD is installed on the top floor of a multi-story timber building, as shown in Figure 14. The dynamic equation of motion of the building equipped with pendulum PTMD under external excitation is developed using the Lagrange method. Theoretical derivation and extensive numerical study of new pendulum PTMD are available in Chapain and Aly’s study [85]. This study modified the equations of single-degree-of-freedom systems for multi-degree-of-freedom systems. The equation of motion of a building with a pendulum PTMD under earthquake excitation is given by:

$$\left. \begin{aligned} (\mathbf{M}_s + \mathbf{L}_d m \mathbf{L}_d^T) \ddot{\mathbf{X}}_s + \mathbf{L}_d m \mathbf{L}_d^T \ddot{\theta} - \mathbf{L}_d m \mathbf{L}_d^T l \dot{\theta}^2 + \mathbf{C}_s \dot{\mathbf{X}}_s + \mathbf{K}_s \mathbf{X}_s &= -\mathbf{M}_s \Lambda \ddot{x}_g - \mathbf{L}_d P \\ I \ddot{\theta} + m \mathbf{L}_d^T l \ddot{\mathbf{X}}_s + c l^2 \dot{\theta} + m l g \theta &= -m \ddot{x}_g + P \end{aligned} \right\} \quad (10)$$

$$I = I_{cm} + m l^2 \quad (11)$$

where \mathbf{M}_s , \mathbf{K}_s , and \mathbf{C}_s are the building’s mass, stiffness, and damping, as previously defined. m is the pendulum mass equal to the equivalent mass of TMD defined in Section 4, l is the pendulum length, θ is the angular displacement of the PTMD, \mathbf{L}_d is the vector containing the damper location, I_{cm} is the moment of inertia of the PTMD, $g = 9.8 \text{ m/s}^2$, and P is the pounding force.

Recently, there has been intense research to model the impact force between adjacent tall buildings under seismic events [86–88]. The linear spring model was used initially to represent the impact force but fails to account for energy dissipation during collision [89]. The Kelvin impact model combines linear spring with a damper, where the damping coefficient is determined to reflect energy dissipation. However, the Kelvin model could not represent the pounding as a highly nonlinear phenomenon. Therefore, an impact model based on Hertz contact law has been suggested lately to include the nonlinear nature of the pounding force [90]. Based on the Hertz law, the pounding force at any given time can be expressed as:

$$P = \begin{cases} \alpha \delta(t)^{\frac{3}{2}} + c(t) \dot{\delta}(t) & \text{for } \delta(t) > 0 \text{ and, } \dot{\delta}(t) > 0 \text{ (Approaching period)} \\ \alpha \delta(t)^{\frac{3}{2}} & \text{for } \delta(t) > 0 \text{ and, } \dot{\delta}(t) < 0 \text{ (Restitution period)} \\ 0 & \text{for } \delta(t) \leq 0 \text{ (No collision)} \end{cases} \quad (12)$$

where $\delta(t)$ is the relative deformation, $\dot{\delta}(t)$ is the impact velocity, α is the pounding stiffness, and $c(t)$ is the damping coefficient resulting from impact.

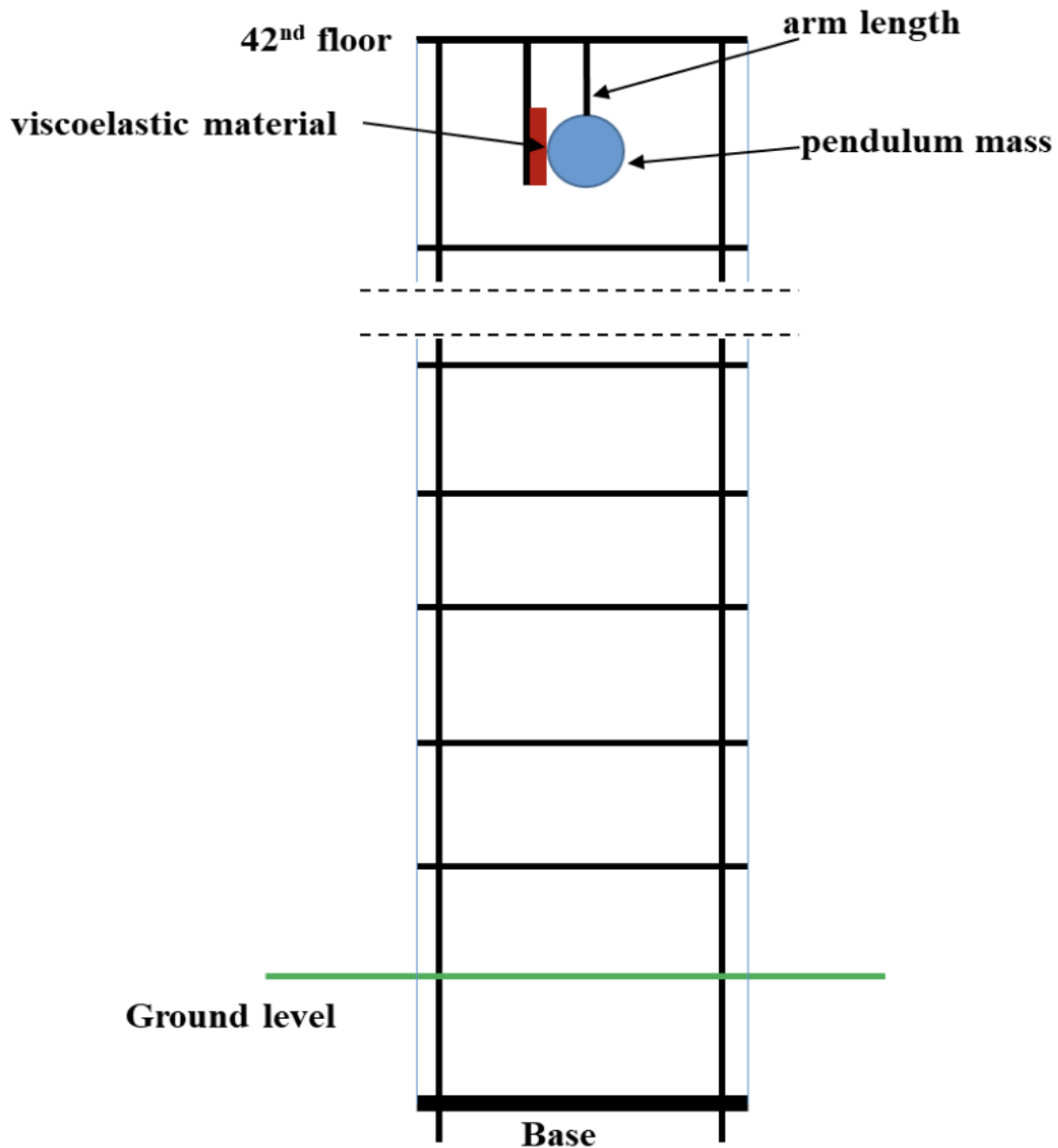


Figure 14. Schematic representation of a high-rise building equipped with a pendulum PTMD.

In the primary impact model, a gap exists between the pounding mass and the viscoelastic boundary [90]. As the viscoelastic material is nonlinear, damping induced by an impact is not uniform; rather, it depends on the structural response. The instantaneous impact damping coefficient is defined as:

$$c(t) = 2\zeta \sqrt{\alpha \sqrt{\delta(t)} \frac{Mm}{M+m}} \tag{13}$$

$$\zeta = \frac{9\sqrt{5}}{2} \frac{1 - e^2}{e(e(9\pi - 16) + 16)} \tag{14}$$

where M and m are the masses of impacting bodies. In this paper, M is considered the first modal mass of the building, and m is the mass of the damper. ζ is the damping ratio

developed from the impact, which relies on the coefficient of restitution e [91]. The frequency of the control device, taking into account pounding duration, can be expressed as:

$$f_{PTMD} = \frac{1}{T} = \frac{1}{\left(\frac{1}{2\pi}\sqrt{\frac{g}{l}} + t_p\right)} \tag{15}$$

If the duration of pounding t_p is insignificant, Equation (15) can be written as:

$$f_{PTMD} = \frac{1}{T} = \frac{1}{2\pi}\sqrt{\frac{g}{l_p}} \tag{16}$$

$$f_R = \frac{f_{PTMD}}{f_1} \tag{17}$$

where f_R is the frequency ratio, l_p is the length of the pendulum arm, and f_1 is the natural frequency of building for the first mode.

8. Performance Comparison among TMD, TMDI, and Pendulum PTMD

In this section, the performance of each control device is investigated and compared under El-Centro earthquake ground acceleration [92]. Unlike wind loads, higher building modes are excited by the seismic loads, so the performance of each control device can be different from the wind. This section uses the optimal parameters of both TMD and TMDI obtained in Section 6 under variable frequency sinusoidal excitations. However, optimal properties of pendulum PTMD are obtained from the previous study [85], where device parameters are optimized under filtered white noise excitations similar to earthquakes. The acceleration spectrum and time history of El-Centro ground acceleration are presented in Figure 15. The peak acceleration is 3.424 m/s^2 , which occurs at 2.12 s (see Figure 15a), with most power concentrated around 1–2 Hz (see Figure 15b). The earthquake has a peak ground velocity of 0.373 m/s, resulting in a PGA/PGV ratio of 9.1.

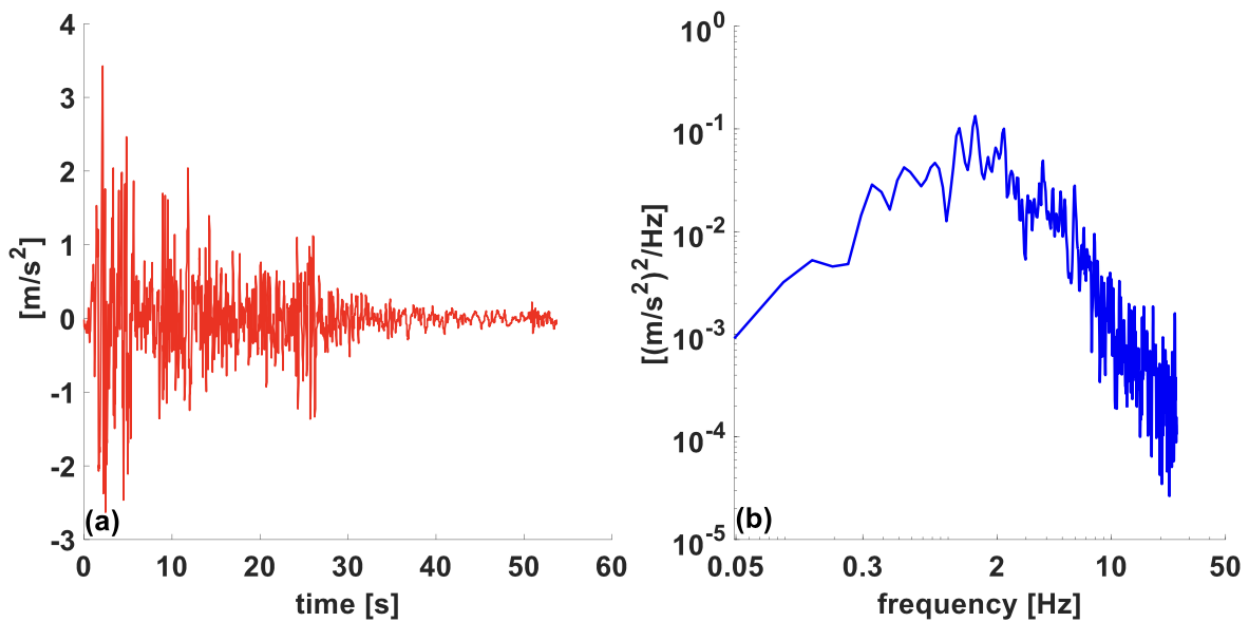


Figure 15. El-Centro earthquake excitation: (a) acceleration time history, and (b) acceleration spectrum.

8.1. Performance Comparison

The pendulum PTMD considerably reduced the displacement and acceleration of the top floor compared to TMD and TMDI (Figure 16). However, displacement responses are reduced more than acceleration responses. The TMDI and TMD were less effective in

controlling the top floor's acceleration, as shown in Figure 16b, although they can reduce the displacement responses, as shown in Figure 16a. Similar to the performance against VF excitations described in Section 6, TMDI is less effective than equivalent TMD under earthquake excitation. Pendulum PTMD reduces the magnitude of excessive vibration and the duration of unwanted vibration, as observed in Figure 16. Responses of the structure under an earthquake in the frequency domain are shown in Figure 17. A significant contribution to displacement response comes from the first mode, but in the case of acceleration, both the first and the second modes contribute. TMD does not reduce higher modes, TMDI has slightly better performance on higher modes, and pendulum PTMD has more success in attenuating higher modes than the other two devices. It should be noticed that both axes in Figure 17 are on a logarithmic scale. Floorwise STD displacements and STD accelerations are presented in Figure 18a,b, respectively. It is observed that pendulum PTMD reduced the displacement at the 42nd floor by 52.9% (STD) and 20% (peak). However, TMD and TMDI decreased the same response by 37.2% (STD), 11.9% (peak), 10.9% (STD), and 4.1% (peak). Although acceleration responses are reduced less in comparison to displacement responses, pendulum PTMD reduces top floor acceleration by 20.5% (STD) and 10.6% (peak), which is much higher compared to the reduction brought by TMD and TMDI.

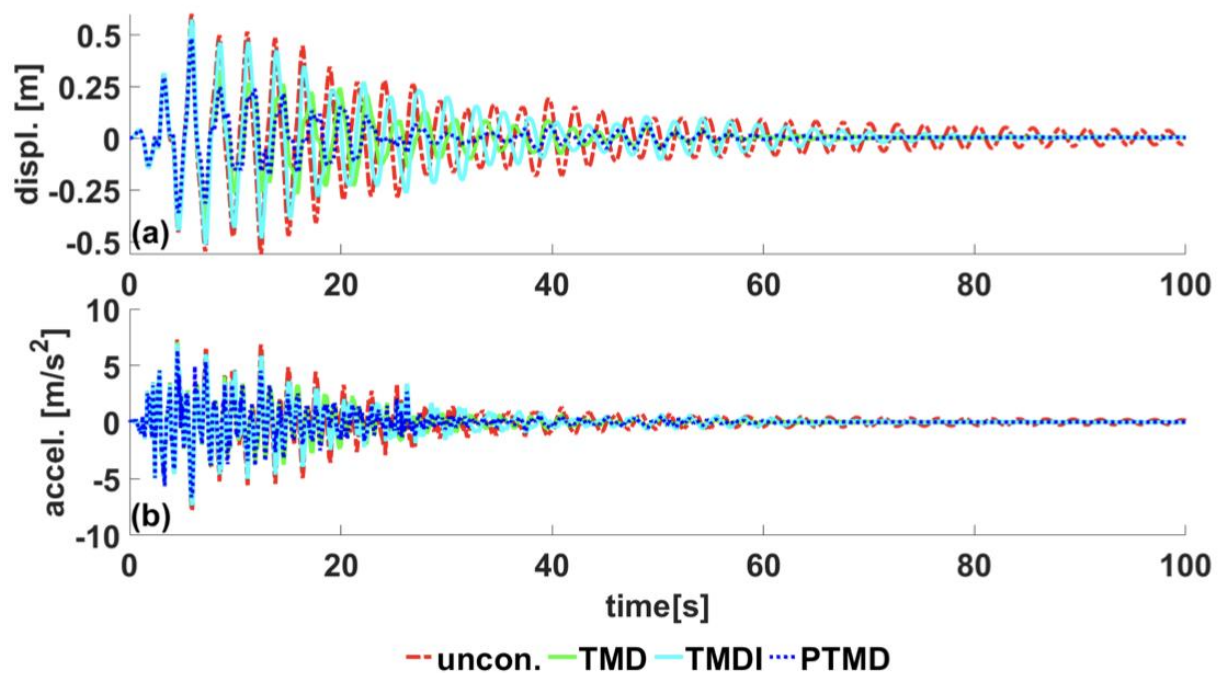


Figure 16. Uncontrolled and controlled displacement and acceleration responses of the 42nd floor, in the time domain, under El-Centro earthquake excitation: (a) displacement response and (b) acceleration response.

Interestingly, the reduction in peak acceleration by TMDI (6.5%) is slightly higher than the TMD (2.6%). This is because TMDI has enhanced control performance than TMD for higher modes, which can be observed from a closer look at Figure 18. This well-known fact supports the result that TMD cannot reduce peak acceleration, which is most often a significant cause of damage and destruction in high-rise buildings during seismic events.

Nevertheless, pendulum PTMD performs better than TMD and TMDI among all modes, including the first mode. Figure 19 presents the floor-wise peak displacement and acceleration of the building. The floor displacement increases linearly over the height of the building, but the acceleration increases non-linearly. This observation shows that higher modes contribute to the acceleration response, and the first mode is dominant in the displacement response.

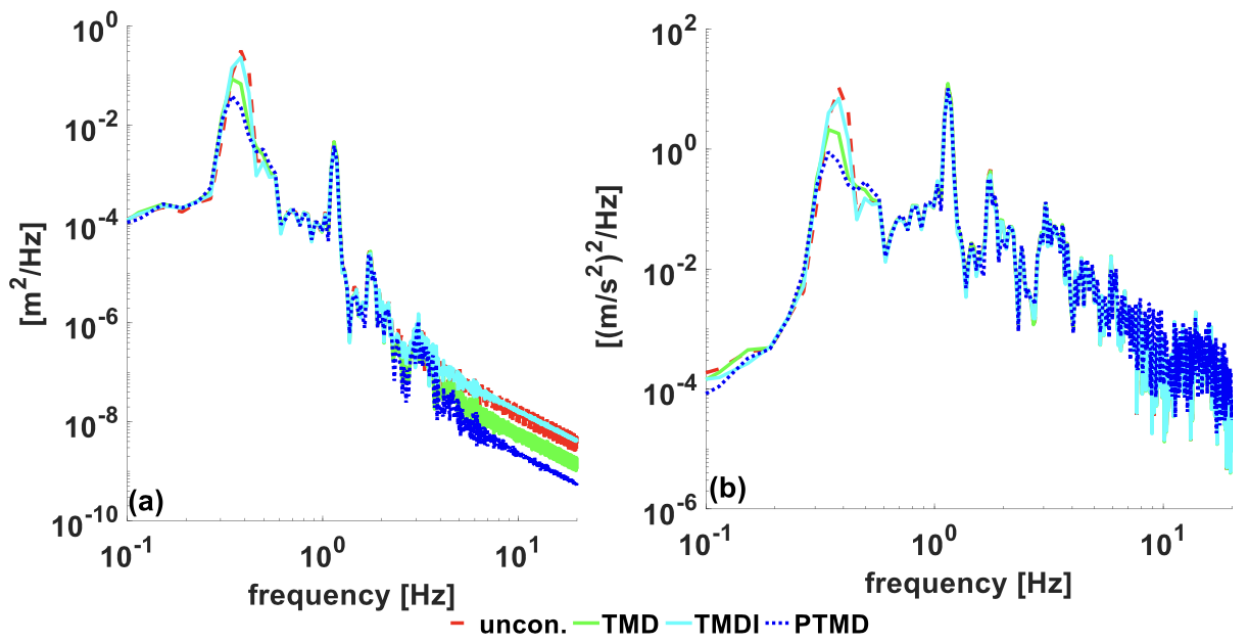


Figure 17. Response spectra of the 42nd story under El-Centro earthquake: (a) displacement and (b) acceleration.

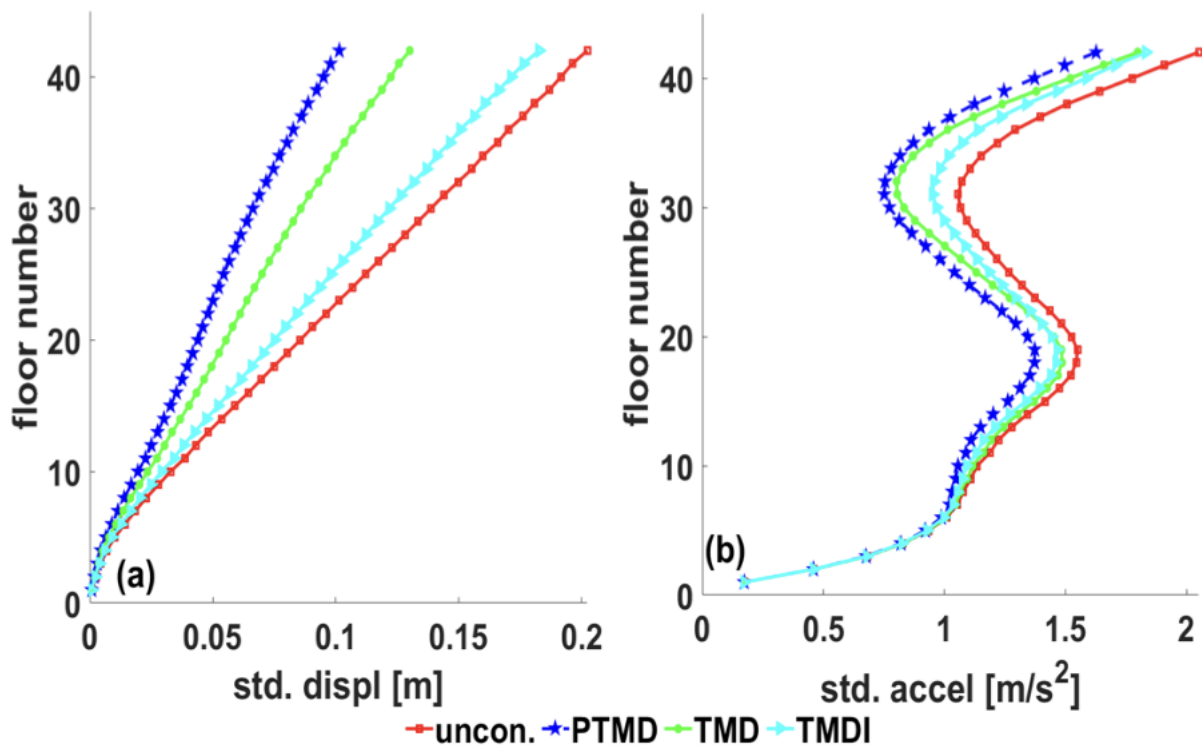


Figure 18. Floorwise responses under El-Centro earthquake: (a) STD displacement, (b) STD acceleration.

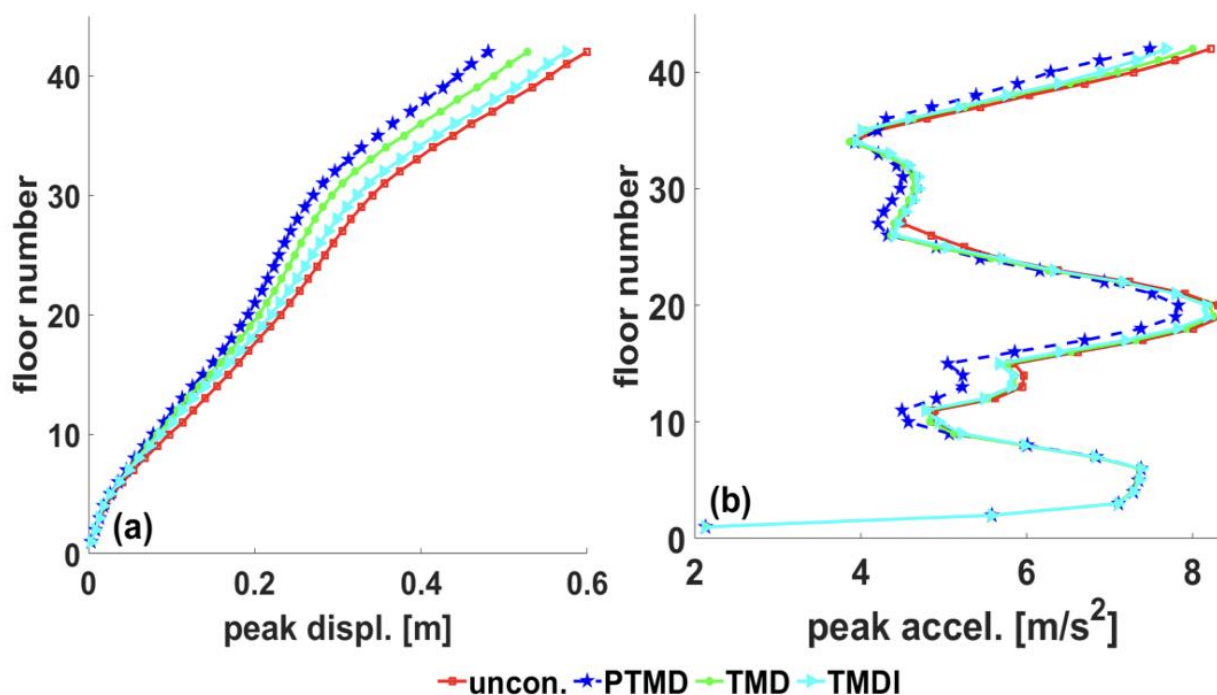


Figure 19. Floorwise responses under El-Centro earthquake: (a) peak displacement, (b) peak acceleration.

Figure 20 shows the shear force on each floor induced by earthquake excitation and the performance comparison of each control device. STD shear at the top is reduced by 22.2% using pendulum PTMD, TMD reduces it by 14%, and TMDI reduces the same response by 11.5%. The performance of both TMD and TMDI is close to reducing both STD and peak shear at the top floor, as described in Figure 20. Considerable reduction in base shear is accomplished using pendulum PTMD over both TMD and TMDI. Nearly 56% reduction in STD base shear is achieved using pendulum PTMD, whereas TMDI and TMD reduce the same response by 33.7% and 47%, respectively. However, a smaller reduction in maximum base shear is obtained compared to STD base shear, as shown in Figure 21. The inter-story drift ratio is a significant performance criterion for the high-rise building under earthquakes. The peak inter-story drift ratio under the El-Centro earthquake is 1.72%. However, the limiting maximum drift ratio for the long-period structure is 2% [93].

Conversely, the 42-story timber building studied in this paper may be safe under moderate seismic excitations, keeping the main force-resisting system in mind. However, nonstructural elements such as ceilings, piping, and partitions may experience considerable damage, resulting in substantial economic loss. Thus, it is crucial to reduce excessive vibration by introducing damping solutions. The pendulum PTMD lowered the peak inter-story drift ratio by 40%. Figure 22 shows the peak inter-story drift ratio and STD drift ratio along with the building's height. Figure 23a shows the STD base moment, and Figure 23b shows the maximum base moment. The pendulum PTMD reduced the STD base moment by 41% and the maximum base moment by 14.5%. The performance of both TMD and TMDI to decrease the base moment is poor compared to the pendulum PTMD, as shown in Figure 23.

8.2. Robustness

The stiffness of the building is considered one of the uncertain parameters. The structure's stiffness may change over time due to material degradation, microtremor, and earthquake excitations. Even though there are several methods and formulations to calculate the stiffness of the building, all procedures have several assumptions that may result in different stiffness of the structure than the actual stiffness in the real world. Thus, it is crucial to investigate the behavior of the control system due to the uncertainty associated

with the stiffness of the building. In this paper, the control performance of TMD, TMDI, and pendulum PTMD is examined by changing the primary stiffness of the whole structure by $\pm 15\%$. The comparative performance of all three devices under the El-Centro earthquake is presented in Table 5. Responses of the uncontrolled building under seismic excitation show that by increasing the structure's stiffness, the displacement response is reduced; however, the acceleration response is increased.

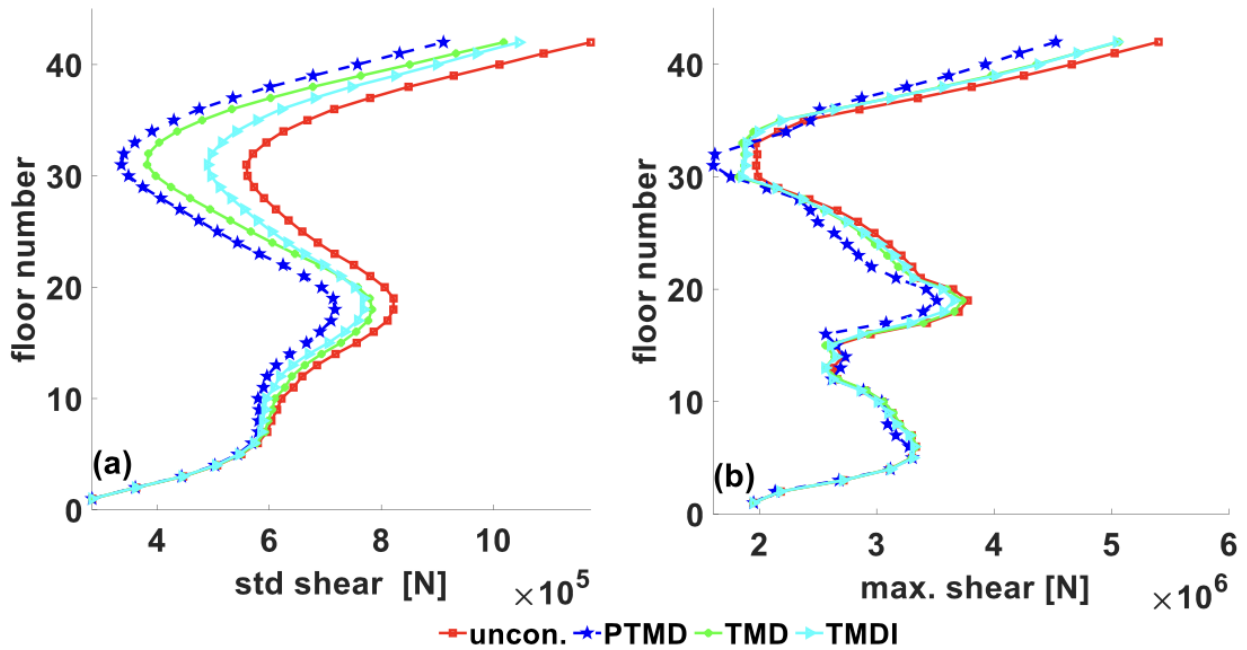


Figure 20. The floorwise shear force under El-Centro earthquake ground acceleration: (a) STD shear, (b) maximum shear.

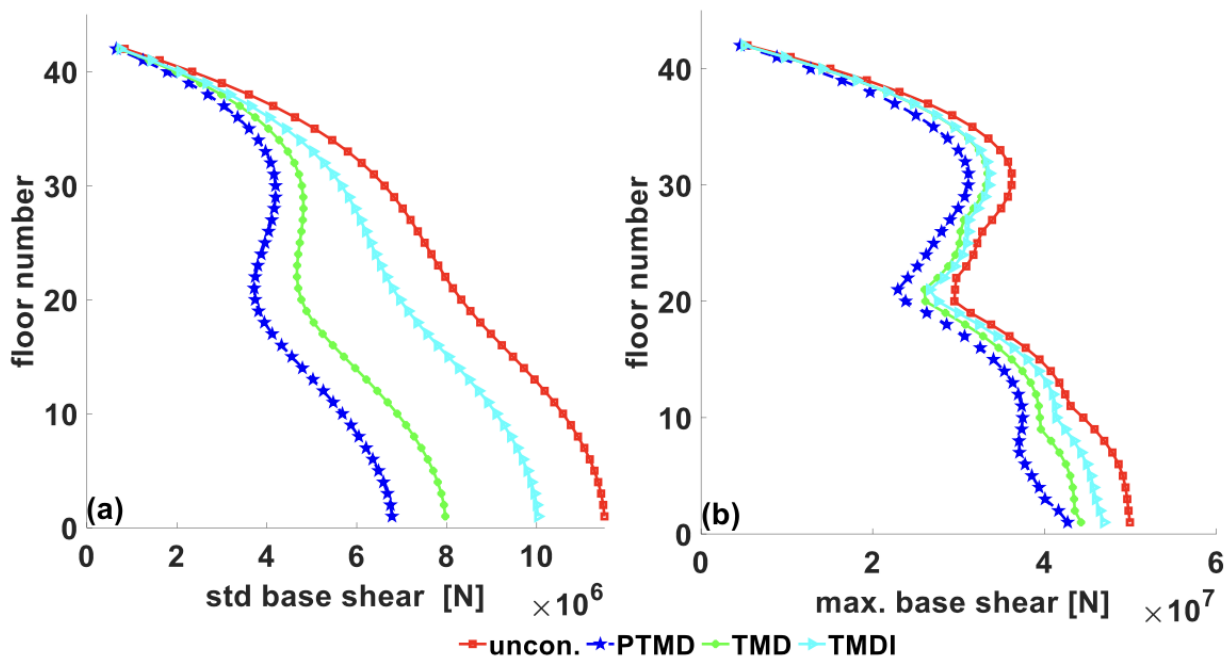


Figure 21. Base shear at each floor: (a) STD shear, (b) maximum shear.

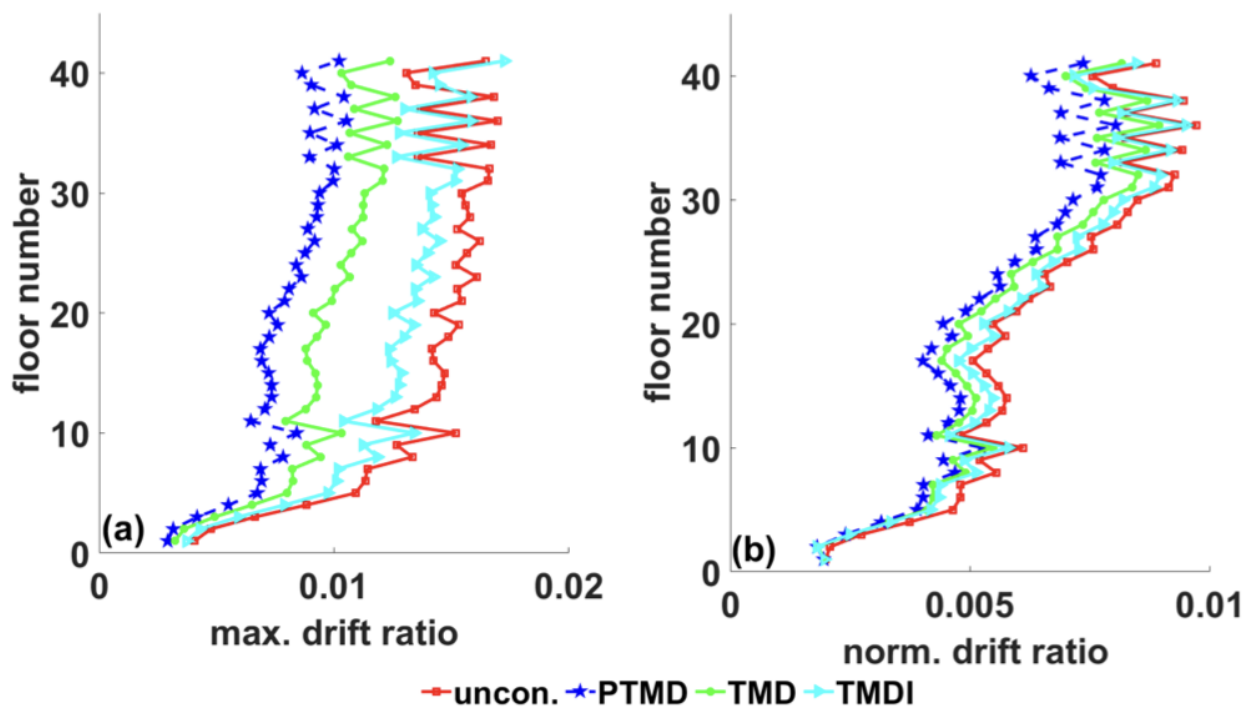


Figure 22. Interstory drift ratio under earthquake: (a) peak drift-ratio, (b) STD drift-ratio.

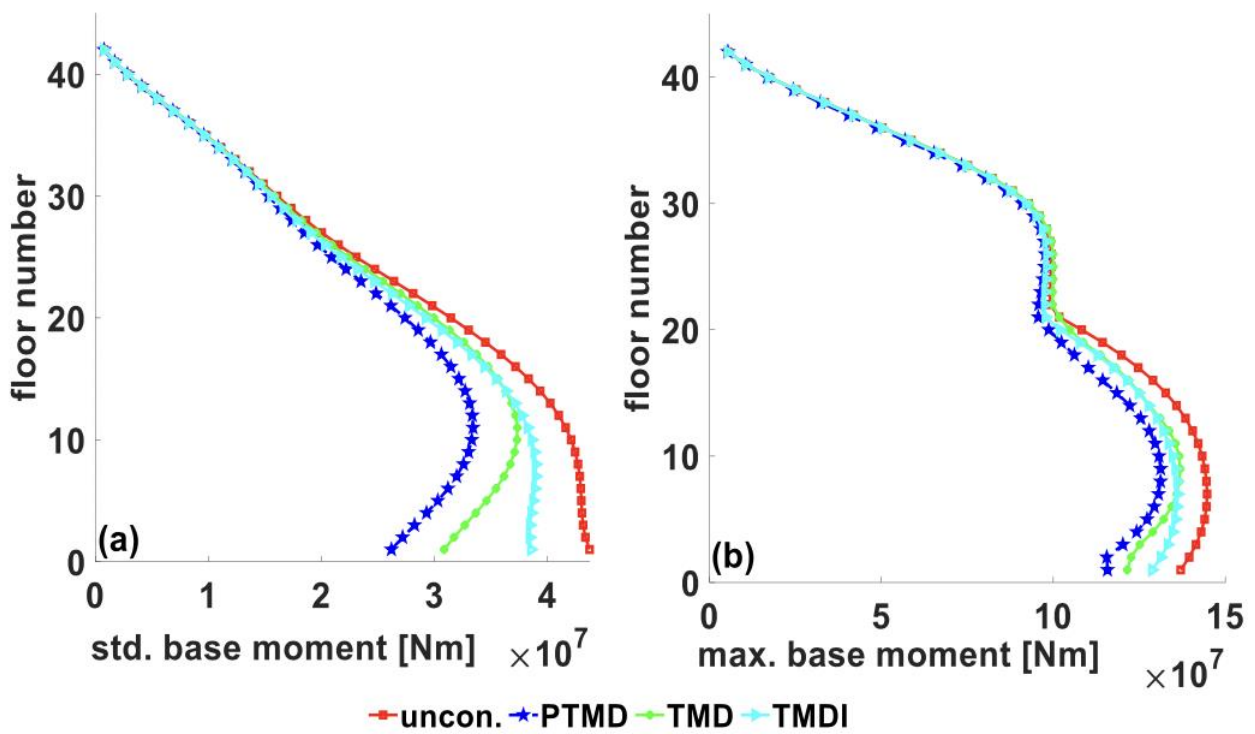


Figure 23. The base moment at each floor: (a) STD moment, (b) maximum moment.

Table 5. The response of the building under El-Centro earthquake ground acceleration with stiffness uncertainty.

Criteria	Uncontrolled			Pendulum PTMD			TMD			TMDI		
	+0% Stiffness	−15% Stiffness	+15% Stiffness	+0% Stiffness	−15% Stiffness	+15% Stiffness	+0% Stiffness	−15% Stiffness	+15% Stiffness	+0% Stiffness	−15% Stiffness	+15% Stiffness
STD dispel. (m)	0.147	0.270	0.140	0.069	0.072	0.055	0.092	0.116	0.069	0.131	0.198	0.089
Peak dispel. (m)	0.599	0.647	0.570	0.482	0.402	0.471	0.528	0.441	0.509	0.575	0.593	0.559
STD accel. (g)	0.149	0.164	0.145	0.118	0.087	0.109	0.129	0.101	0.114	0.132	0.127	0.119
Peak accel. (g)	0.836	0.797	0.858	0.749	0.723	0.717	0.815	0.765	0.769	0.782	0.742	0.808
STD base shear (N)	1.510×10^7	1.597×10^7	1.192×10^7	6.785×10^6	5.253×10^6	6.692×10^6	7.969×10^6	7.056×10^6	7.040×10^6	1.003×10^7	1.115×10^7	8.440×10^6
Peak base Shear (N)	4.994×10^7	4.848×10^7	5.257×10^7	4.271×10^7	4.420×10^7	4.350×10^7	4.425×10^7	4.356×10^7	4.577×10^7	4.691×10^7	4.485×10^7	5.073×10^7
STD base moment (N.m)	3.157×10^7	4.380×10^7	3.271×10^7	1.861×10^7	1.441×10^7	1.726×10^7	2.186×10^7	1.935×10^7	1.931×10^7	2.750×10^7	3.059×10^7	2.315×10^7
Peak base moment (N.m)	1.371×10^8	1.329×10^8	1.443×10^8	1.172×10^8	1.213×10^8	1.194×10^8	1.215×10^8	1.196×10^8	1.256×10^8	1.287×10^8	1.231×10^8	1.392×10^8
STD drift ratio (%)	0.80	0.70	0.81	0.73	0.53	0.68	0.81	0.60	0.74	0.84	0.83	0.78
Peak drift ratio (%)	1.72	2.88	1.55	1.02	0.96	0.74	1.26	1.44	0.88	1.59	2.59	1.04

Similarly, decreasing the building stiffness increases the displacement response while peak acceleration is reduced. It is observed that the proposed pendulum PTMD has much better potential to reduce responses of the building considering the stiffness uncertainty. Displacement, acceleration, base shear, base moment, and drift ratio are reduced more by pendulum PTMD than TMD and TMDI when the stiffness of the building is changed by $\pm 15\%$. The control performance of the pendulum PTMD remains almost the same. However, the performance of TMD and TMDI is reduced significantly due to detuning. This observation demonstrates the robustness of pendulum PTMD. It can address the challenges of physical civil infrastructure to be resilient and sustainable over its service lifetime, under service and long-term conditions, including increased demands due to climate change adaptation and other emerging stressors (including single and multiple hazard events).

8.3. Prevention of Local Damage and Impact Noise Reduction

Figure 24 presents the pounding force under El-Centro excitation. Initially, the pounding force was smaller because the magnitude of excitation was small. Later, with increased excitation magnitude, the pounding force also increased and peaked at 106 N. During seismic events, the magnitude of the pounding force can be excessively high, causing local damage to the pounding area. Therefore, it is essential to implement a protection technique to prevent local damage at the pounding surface. There has been an extensive study to minimize the damage caused by structural pounding, especially in adjacent tall buildings during seismic excitations [94]. Local damage brought by the pounding force can be minimized by dispensing the concentrated pounding force over a large surface area. A secondary structural member having a trapezoidal shape can be introduced between the viscoelastic material and the building so that the pounding force per unit area on the building is reduced. The rectangular plate attached to viscoelastic material, as shown in Figure 14, transfers the pounding force to the building floor. The concentration of pounding force can also be reduced by connecting the rectangular plate to the core of the building so that local damage can be prevented.

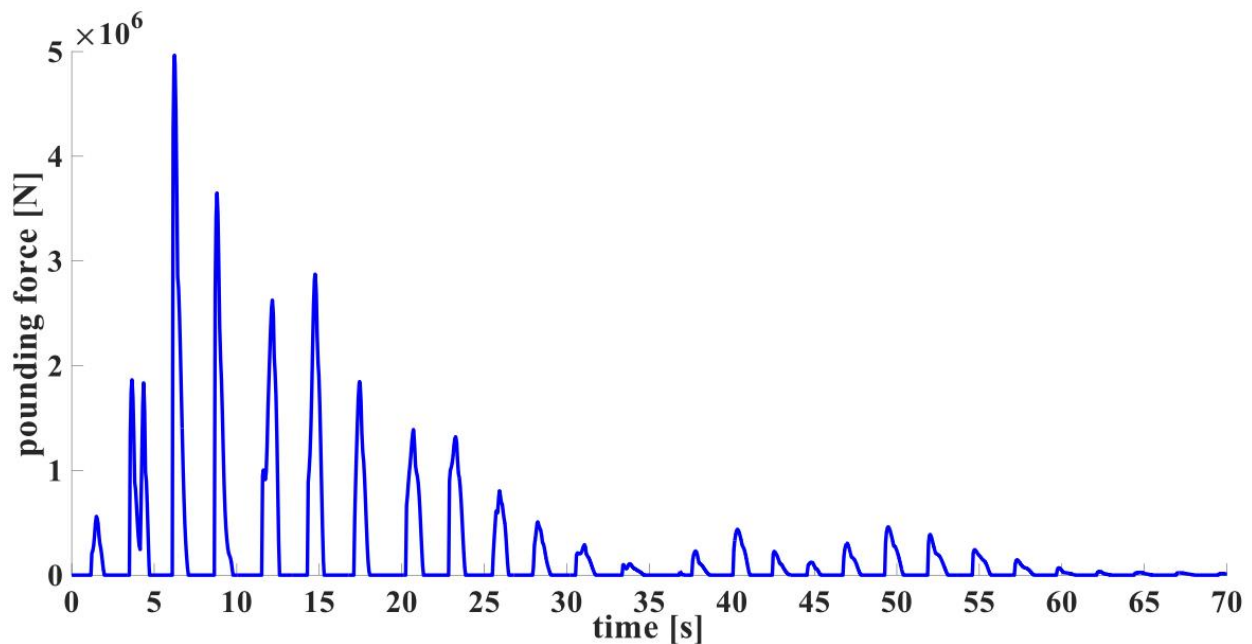


Figure 24. The pounding force under El-Centro earthquake excitation.

Despite its potential to control vibrations under natural hazards, implementing the pendulum PTMD in real life may have issues with noise from the impact mass. The pendulum PTMD under wind loads could produce noise that may result in human discomfort or even problems with hearing loss when exposed for an extended period [95]. There have been several studies on impact noise control in mechanical devices and during the construction of civil engineering structures [96,97]. In the case of PTMD impact noise, a simple enclosure can be installed on the impact area with acoustic materials such as perforated plywood or fibrous plaster.

9. Conclusions

This paper aims to evaluate the performance of the TMD, TMDI, and the pendulum PTMD to reduce excessive vibrations in a 42-story hybrid timber building. The outcomes of the study are summarized as follows.

- A proposed robust pendulum PTMD with the same mass ratio as TMD and TMDI offers an excellent vibration reduction due to its superior energy dissipation at the pounding boundary. Under earthquake excitations, the proposed device can reduce the peak displacement at the top floor by 19.5%, while the TMD reduces the same response by 11.9%, and the TMDI reduces the response by 4.1%. In addition, the pendulum PTMD reduces top floor acceleration by 11%, while the TMD reduces it by a negligible amount. The robustness of the pendulum PTMD is superior compared to TMD/TMDI.
- The pendulum PTMD reduced the base shear force by 55.7% (STD) and 14.5% (peak value), the base moment by 41% (STD) and 14% (peak value), and the maximum inter-story drift ratio by 40% (peak value). The superior performance of the proposed pendulum PTMD in reducing peak accelerations reveals that the device can minimize damage to the building's nonstructural elements (pipes, ceiling, partitions, etc.) during seismic events.
- An equivalent TMD, including the physical mass of the inerter, is proposed for a one-to-one performance comparison between TMD and TMDI. The introduction of the inerter in a linear TMD may change the optimal device properties (damping ratio and tuning frequency, resulting in reduced energy dissipation). The results show that the equivalent

TMD is better than TMDI in minimizing the building responses under variable frequency sinewave excitations unless the mass ratio is significantly small (<0.005).

- The three devices can minimize acceleration better (compared to displacement) under filtered white noise (wind loads). However, the opposite is true under a variable frequency sinewave excitation (earthquake excitation). Nevertheless, due to the nonlinear behavior of the pendulum PTMD, higher modes are controlled, which results in a higher reduction in the acceleration response.
- The control capabilities of the TMD increase with the increase in the mass ratio. However, the responses are sensitive to small mass ratios (0–2%). Similarly, for a given mass ratio, the vibration reduction capabilities of the TMDI increase as the inertance ratio increases. The structural responses are sensitive to the inertance ratio within the range of 0–0.5. Increasing the inertance ratio beyond 0.5 is inefficient and increases the device's physical mass.
- Pendulum PTMD has a potential application against multi-hazard (wind/earthquake) loads, resulting in sustainable and resilient future infrastructures. It can address the challenges of physical civil infrastructure to be resilient and sustainable over its service lifetime, under service and long-term conditions, including increased demands due to climate change adaptation and other emerging stressors (including single and multiple hazard events).

The dominant capabilities of this novel device in a timber-hybrid building under different excitations reveal benefits that can shape the future of the physical infrastructure and contribute to climate change adaptation and mitigation for improved disaster resilience. In addition, these findings can contribute to fostering community welfare and promoting environmentally friendly, circular economy policies.

Author Contributions: Conceptualization, A.M.A.; Methodology, S.C. and A.M.A.; Writing—original draft, S.C. and A.M.A.; Funding acquisition, A.M.A. All authors have read and agreed to the published version of the manuscript.

Funding: The second author (A.M. Aly) received funds from the Louisiana Board of Regents (ITRS program: LEQSF(2022-25)-RD-B-02), Louisiana State University (LSU) NSF I-Corps, LSU Faculty Grant, as well as LSU Economic Development Assistantships (EDAs) through the NSF EPSCoR program. The findings are those of the authors and do not necessarily represent the sponsors' views.

Institutional Review Board Statement: Not applicable.

Informed Consent Statement: Not applicable.

Data Availability Statement: Not applicable.

Conflicts of Interest: The authors declare no competing interests.

References

1. Poirier, E.; Moudgil, M.; Fallahi, A.; Staub-French, S.; Tannert, T. Design and construction of a 53-meter-tall timber building at the University of British Columbia. In Proceedings of the World Conference on Timber Engineering, Vienna, Austria, 22–25 August 2016.
2. Stepinac, M.; Šušteršič, I.; Gavrić, I.; Rajčić, V. Seismic design of timber buildings: Highlighted challenges and future trends. *Appl. Sci.* **2020**, *10*, 1380. [[CrossRef](#)]
3. Morrison, M.J.; Kopp, G.A. performance of toe-nail connections under realistic wind loading. *Eng. Struct.* **2011**, *33*, 69–76. [[CrossRef](#)]
4. He, J.; Pan, F.; Cai, C.S. A review of wood-frame low-rise building performance study under hurricane winds. *Eng. Struct.* **2017**, *141*, 512–529. [[CrossRef](#)]
5. Somayaji, S. Low-rise timber buildings subjected to seismic wind and snow loads. *J. Struct. Eng.* **1985**, *111*, 1164–1166. [[CrossRef](#)]
6. Rosowsky, D.; Schiff, S. What are our expectations, objectives, and performance requirements for wood structures in high wind regions? *Nat. Hazards Rev.* **2003**, *4*, 144–148. [[CrossRef](#)]
7. Mensah, A.F.; Datin, P.L.; Prevatt, D.O.; Gupta, R.; van de Lindt, J.W. Database-assisted design methodology to predict wind-induced structural behavior of a light-framed wood building. *Eng. Struct.* **2011**, *33*, 674–684. [[CrossRef](#)]
8. Schober, K.U.; Tannert, T. Hybrid connections for timber structures. *Eur. J. Wood Wood Prod.* **2016**, *74*, 369–377. [[CrossRef](#)]
9. Branco, J.M.; Piazza, M.; Cruz, P.J.S. Experimental evaluation of different strengthening techniques of traditional timber connections. *Eng. Struct.* **2011**, *33*, 2259–2270. [[CrossRef](#)]

10. Tesfamariam, S.; Stiemer, S.F. Special issue on performance of timber and hybrid structures. *J. Perform. Constr. Facil.* **2014**, *28*, 1–3. [[CrossRef](#)]
11. Kocan, C.; Özgen, G.O. Investigation of the effect of structural damping on wind turbine wind-induced fatigue loads. *Mech. Based Des. Struct. Mach.* **2022**, 1–26. [[CrossRef](#)]
12. Huber, J.A.J.; Ekevad, M.; Girhammar, U.A.; Berg, S. Structural robustness and timber buildings—A review. *Wood Mater. Sci. Eng.* **2019**, *14*, 107–128. [[CrossRef](#)]
13. Xie, Z.; Hu, X.; Du, H.; Zhang, X. Vibration behavior of timber-concrete composite floors under human-induced excitation. *J. Build. Eng.* **2020**, *32*, 101744. [[CrossRef](#)]
14. Chapain, S.; Aly, A.M. Vibration attenuation in high-rise buildings to achieve system-level performance under multiple hazards. *Eng. Struct.* **2019**, *197*, 109352. [[CrossRef](#)]
15. Khatibinia, M.; Gholami, H.; Kamgar, R. Optimal design of tuned mass dampers subjected to continuous stationary critical excitation. *Int. J. Dyn. Control* **2018**, *6*, 1094–1104. [[CrossRef](#)]
16. Jeong, S.Y.; Kang, T.H.-K.; Yoon, J.K.; Klemencic, R. Seismic performance evaluation of a tall building: Practical modeling of surrounding basement structures. *J. Build. Eng.* **2020**, *31*, 101420. [[CrossRef](#)]
17. Beskhyroun, S.; Navabian, N.; Wotherspoon, L.; Ma, Q. Dynamic behaviour of a 13-story reinforced concrete building under ambient vibration, forced vibration, and earthquake excitation. *J. Build. Eng.* **2020**, *28*, 101066. [[CrossRef](#)]
18. Fragiaco, M.; Dujic, B.; Sustersic, I. Elastic and ductile design of multi-storey crosslam massive wooden buildings under seismic actions. *Eng. Struct.* **2011**, *33*, 3043–3053. [[CrossRef](#)]
19. Tassios, T.P. *Seismic Design of Reinforced Concrete and Masonry Buildings*; Wiley: New York, NY, USA, 1993; Volume 12.
20. Pacchioli, S.; Pozza, L.; Trutalli, D.; Polastri, A. Earthquake-resistant CLT buildings stiffened with vertical steel ties. *J. Build. Eng.* **2021**, *40*, 102334. [[CrossRef](#)]
21. Gavric, I.; Fragiaco, M.; Ceccotti, A. Cyclic behavior of CLT wall systems: Experimental tests and analytical prediction models. *J. Struct. Eng.* **2015**, *141*, 04015034. [[CrossRef](#)]
22. Igor, G.; Massimo, F.; Ario, C. Strength and deformation characteristics of typical X-lam connections. In Proceedings of the World Conference on Timber Engineering 2012, WCTE 2012, Auckland, New Zealand, 15–19 July 2012; pp. 146–155. Available online: http://support.sbcindustry.com/Archive/2012/july/Paper_092.pdf (accessed on 4 February 2023).
23. Ceccotti, A.; Follesa, M.; Lauriola, M.P.; Sandhaas, C. Sofie Project—Test Results on the Lateral Resistance of Cross-Laminated Wooden Panels. In Proceedings of the First European Conference on Earthquake Engineering and Seismicity, Geneva, Switzerland, 3–8 September 2006; p. 10. Available online: http://www.timberengineering.it/Pubblicazioni/img/Articoli_scientifici/2006_ECEES_Testresults.pdf (accessed on 4 February 2023).
24. Baker, J.W. Measuring bias in structural response caused by ground motion scaling. In Proceedings of the 8th Pacific Conference on Earthquake Engineering, Singapore, 5–7 December 2007; pp. 1–6. [[CrossRef](#)]
25. Popovski, M.; Gavric, I. Performance of a 2-Story CLT House Subjected to Lateral Loads. *J. Struct. Eng.* **2016**, *142*, 1–12. [[CrossRef](#)]
26. Reynolds, T.; Harris, R.; Chan, W.S. Dynamic response of tall timber buildings to wind load. In Proceedings of the 35th Annual Symposium of IABSE/52nd Annual Symposium of IASS/6th International Conference on Space Structures, London, UK, 20–23 September 2011.
27. Bezabeh, M.A.; Bitsuamlak, G.T.; Popovski, M.; Tesfamariam, S. Probabilistic serviceability-performance assessment of tall mass-timber buildings subjected to stochastic wind loads: Part I—Structural design and wind tunnel testing. *J. Wind Eng. Ind. Aerodyn.* **2018**, *181*, 85–103. [[CrossRef](#)]
28. Bezabeh, M.A.; Gairola, A.; Bitsuamlak, G.T.; Popovski, M.; Tesfamariam, S. Structural performance of multi-story mass-timber buildings under tornado-like wind field. *Eng. Struct.* **2018**, *177*, 519–539. [[CrossRef](#)]
29. Johansson, M.; Linderholt, A.; Jarnerö, K.; Landel, P. Tall timber buildings—A preliminary study of wind-induced vibrations of a 22-storey building. In Proceedings of the World Conference on Timber Engineering (WCTE 2016), Vienna, Austria, 22–25 August 2016.
30. Dadkhaha, M.; Kamgar, R.; Heidarzadeh, H. Reducing the Cost of Calculations for Incremental Dynamic Analysis of Building Structures Using the Discrete Wavelet Transform. *Eng. J. Earthq. Eng.* **2022**, *26*, 3317–3342. [[CrossRef](#)]
31. Skidmore Owings and Merrill (SOM LLP). *Timber Tower Research Project*; Skidmore Owings and Merrill (SOM LLP): Chicago, IL, USA, 2013.
32. *Manual for Engineered Wood Construction*; American Wood Council: Leesburg, VA, USA, 2018.
33. van de Kuilen, J.W.G.; Ceccotti, A.; Xia, Z.; He, M. Very tall wooden buildings with Cross Laminated Timber. *Procedia Eng.* **2011**, *14*, 1621–1628. [[CrossRef](#)]
34. Zhang, X. Seismic Design of Timber Steel Hybrid High-Rise Buildings. Ph.D. Thesis, University of British Columbia, Vancouver, BC, Canada, 2017.
35. Karacabeyli, E.; Brad, D. *Hand Book Cross Laminated Timber*; SP-529E; FPIInnovations, Spec. Publ.: Leesburg, VA, USA, 2013; p. 572. Available online: https://cdn2.hubspot.net/hubfs/5577290/PDFs/CLT%20Handbook/CLT_USA-Complete-document-Think_Wood.pdf (accessed on 4 February 2023).
36. Tamura, Y.; Akihito, Y. Amplitude Dependency of Damping in Buildings. In Proceedings of the Structures Congress 2008: 18th Analysis and Computation Speciality Conference, Vancouver, BC, Canada, 24–26 April 2008.

37. Aly, A.M. Pressure integration technique for predicting wind-induced response in high-rise buildings. *Alex. Eng. J.* **2013**, *52*, 717–731. [[CrossRef](#)]
38. Chowdhury, I.; Dasgupta, S.P. Computation of Rayleigh damping coefficients for large systems. *Electron. J. Geotech. Eng.* **2003**, *8*, 1–11.
39. Housner, G.W.; Bergman, L.A.; Caughey, T.K.; Chassiakos, A.G. Structural control: Past, present, and future. *J. Eng. Mech.* **1997**, *123*, 897–971. [[CrossRef](#)]
40. Spencer, B.F.J.; Nagarajah, S. State of the Art of Structural Control. *J. Struct. Eng.* **2003**, *129*, 845–846. [[CrossRef](#)]
41. Tanveer, M.; Usman, M.; Khan, I.U.; Farooq, S.H.; Hanif, A. Material optimization of tuned liquid column ball damper (TLCBD) for the vibration control of multi-storey structure using various liquid and ball densities. *J. Build. Eng.* **2020**, *32*, 101742. [[CrossRef](#)]
42. Reiterer, M.; Schellander, J. A Novel Single Tube Semi-Active Tuned Liquid Gas Damper for Suppressing Horizontal Vibrations of Tower-like Structures. *Appl. Sci.* **2022**, *12*, 3301.
43. Bigdeli, Y.; Kim, D. Damping effects of the passive control devices on structural vibration control: TMD, TLC and TLCD for varying total masses. *KSCE J. Civ. Eng.* **2016**, *20*, 301–308. [[CrossRef](#)]
44. Bigdeli, Y.; Kim, D. Response control of irregular structures using structure-TLCD coupled system under seismic excitations. *KSCE J. Civ. Eng.* **2015**, *19*, 672–681. [[CrossRef](#)]
45. Bigdeli, Y.; Kim, D.; Chang, S. Vibration control of 3D irregular buildings by using developed neuro-controller strategy. *Struct. Eng. Mech.* **2014**, *49*, 687–703. [[CrossRef](#)]
46. Dadkhah, M.; Kamgar, R.; Heidarzadeh, H.; Jakubczyk-Galczyńska, A.; Jankowski, R. Improvement of Performance Level of Steel Moment-Resisting Frames Using Tuned Mass Damper System. *Appl. Sci.* **2020**, *10*, 3403. [[CrossRef](#)]
47. Nakano, Y.; Kishi, T.; Takahara, H. Experimental Study on Application of Tuned Mass Dampers for Chatter in Turning of a Thin-Walled Cylinder. *Appl. Sci.* **2021**, *11*, 12070. [[CrossRef](#)]
48. Aksoy, T.; Özgen, G.O.; Acar, B. Design of a tuned vibration absorber for a slender hollow cylindrical structure. *Mech. Based Des. Struct. Mach.* **2020**, *48*, 615–648. [[CrossRef](#)]
49. Longarini, N.; Cabras, L.; Zucca, M.; Chapain, S.; Aly, A.M. Structural Improvements for Tall Buildings under Wind Loads: Comparative Study. *Shock Vib.* **2017**, *2017*, 2031248. [[CrossRef](#)]
50. Abdelnaeem, M.; Elsouhily, B.; Elgamal, H. Multi Objective Optimization of a Quarter Car Model Fitted with an MR-Damper. *Int. J. Adv. Mech. Aeronaut. Eng.* **2018**, *5*, 7–13.
51. Basili, M.; de Angelis, M. Experimental Dynamic Response of a Multi-Story Frame Structure Equipped with Non-Conventional TMD Implemented via Inter-Story Isolation. *Appl. Sci.* **2022**, *12*, 9153. [[CrossRef](#)]
52. Ozturk, B.; Cetin, H.; Dutkiewicz, M.; Aydin, E.; Farsangi, E.N. On the Efficacy of a Novel Optimized Tuned Mass Damper for Minimizing Dynamic Responses of Cantilever Beams. *Appl. Sci.* **2022**, *12*, 7878. [[CrossRef](#)]
53. Ghoniem, M.; Awad, T.; Mokhiamar, O. Control of a new low-cost semi-active vehicle suspension system using artificial neural networks. *Alex. Eng. J.* **2020**, *59*, 4013–4025. [[CrossRef](#)]
54. Kareem, A.; Kijewski, T.; Tamura, Y. Mitigation of motions of tall buildings with specific examples of recent applications. *Wind Struct. An Int. J.* **1999**, *2*, 201–251. [[CrossRef](#)]
55. Aly, A.M. Proposed robust tuned mass damper for response mitigation in buildings exposed to multidirectional wind. *Struct. Des. Tall Spec. Build.* **2014**, *23*, 664–691. [[CrossRef](#)]
56. Salimi, M.; Kamgar, R.; Heidarzadeh, H. An evaluation of the advantages of friction TMD over conventional TMD. *Innov. Infrastruct. Solut.* **2021**, *6*, 95. [[CrossRef](#)]
57. Martinez-Paneda, M.; Elghazouli, A.Y. An integrated damping system for tall buildings. *Struct. Des. Tall Spec. Build.* **2020**, *29*, e1724. [[CrossRef](#)]
58. Kamgar, R.; Gholami, F.; Sanayei, H.R.Z.; Heidarzadeh, H. Modified Tuned Liquid Dampers for Seismic Protection of Buildings Considering Soil–Structure Interaction Effects. *Iran. J. Sci. Technol. Trans. Civ. Eng.* **2020**, *44*, 339–354. [[CrossRef](#)]
59. Guan, D.; Cong, X.; Li, J.; Wang, P.; Yang, Z.; Jing, X. Theoretical modeling and optimal matching on the damping property of mechatronic shock absorber with low speed and heavy load capacity. *J. Sound Vib.* **2022**, *535*, 117113. [[CrossRef](#)]
60. Jafari, M.; Alipour, A. Methodologies to mitigate wind-induced vibration of tall buildings: A state-of-the-art review. *J. Build. Eng.* **2021**, *33*, 101582. [[CrossRef](#)]
61. Weber, F.; Borchsenius, F.; Distl, J.; Braun, C. Performance of Numerically Optimized Tuned Mass Damper with Inerter (TMDI). *Appl. Sci.* **2022**, *12*, 6204.
62. Marian, L.; Giaralis, A. Optimal design of a novel tuned mass-damper-inerter (TMDI) passive vibration control configuration for stochastically support-excited structural systems. *Probabilistic Eng. Mech.* **2014**, *38*, 156–164. [[CrossRef](#)]
63. Petrini, F.; Giaralis, A.; Wang, Z. Optimal tuned mass-damper-inerter (TMDI) design in wind-excited tall buildings for occupants' comfort serviceability performance and energy harvesting. *Eng. Struct.* **2020**, *204*, 109904. [[CrossRef](#)]
64. Smith, M.C. Synthesis of mechanical networks: The inerter. *IEEE Trans. Automat. Contr.* **2002**, *47*, 1648–1662. [[CrossRef](#)]
65. Papageorgiou, C.; Smith, M.C. Laboratory experimental testing of inerters. In Proceedings of the 44th IEEE Conference on Decision and Control, Seville, Spain, 15 December 2005; pp. 3351–3356. [[CrossRef](#)]
66. Chen, M.Z.Q.; Hu, Y. *Inerter and Its Application in Vibration Control Systems*; Springer: Singapore, 2019; pp. 1–122. [[CrossRef](#)]
67. Nakaminami, S.; Kida, H.; Ikago, K.; Inoue, N. Dynamic testing of a full-scale hydraulic inerter-damper for the seismic protection of civil structures. In Proceedings of the 7th International Conference on Advances in Experimental Structural Engineering, AESE 2017, Pavia, Italy, 6–8 September 2017; pp. 41–54. [[CrossRef](#)]

68. Smith, M.C. Performance Benefits in Passive Vehicle Suspensions Employing Inerters. *Taylor Fr.* **2004**, *42*, 235–257. [CrossRef]
69. Caicedo, D.; Lara-Valencia, L.; Blandon, J.; Graciano, C. Seismic response of high-rise buildings through metaheuristic-based optimization using tuned mass dampers and tuned mass dampers inerter. *J. Build. Eng.* **2021**, *34*, 101927. [CrossRef]
70. Madhamshetty, K.; Manimala, J.M. Low-rate characterization of a mechanical inerter. *Machines* **2018**, *6*, 32. [CrossRef]
71. Wang, Q.; Qiao, H.; de Domenico, D.; Zhu, Z.; Xie, Z. Wind-induced response control of high-rise buildings using inerter-based vibration absorbers. *Appl. Sci.* **2019**, *9*, 5045. [CrossRef]
72. de Domenico, D.; Ricciardi, G. An enhanced base isolation system equipped with optimal tuned mass damper inerter (TMDI). *Earthq. Eng. Struct. Dyn.* **2018**, *47*, 1169–1192. [CrossRef]
73. Attaway, S. *MATLAB: A Practical Introduction to Programming and Problem Solving*, 5th ed.; Butterworth-Heinemann: Woburn, MA, USA, 2018.
74. Liberty, S.; Ogata, K.; Liberty, S. *Modern Control Engineering*; Elsevier: Amsterdam, The Netherlands, 1972; Volume 17.
75. Li, Q.S.; Zhi, L.H.; Tuan, A.Y.; Kao, C.S.; Su, S.C.; Wu, C.F. Dynamic behavior of Taipei 101 tower: Field measurement and numerical analysis. *J. Struct. Eng.* **2011**, *137*, 143–155. [CrossRef]
76. Mazza, F.; Sininno, S. Nonlinear dynamic behavior of base-isolated buildings with the friction pendulum system subjected to near-fault earthquakes. *Mech. Based Des. Struct. Mach.* **2017**, *45*, 331–344.
77. Zhang, P.; Song, G.; Li, H.N.; Lin, Y.X. Seismic control of power transmission tower using pounding TMD. *J. Eng. Mech.* **2013**, *139*, 1395–1406. [CrossRef]
78. Song, G.B. Vibration control of a pipeline structure using pounding tuned mass damper. *J. Eng. Mech.* **2016**, *142*, 04016031. [CrossRef]
79. Patil, D.; Kalia, A.; Ho, S.C.M.; Zhang, P.; Lara, M.; Song, G. Pounding Tuned Mass Damper (PTMD): An innovative damper for subsea pipeline and jumper vibration controls. In Proceedings of the Offshore Mediterranean Conference and Exhibition, Ravenna, Italy, 29–March 2017; pp. 1–11. [CrossRef]
80. Li, H.; Zhang, P.; Song, G.; Patil, D.; Mo, Y. Robustness study of the pounding tuned mass damper for vibration control of subsea jumpers. *Smart Mater. Struct.* **2015**, *24*, 095001. [CrossRef]
81. Zhang, P.; Li, L.; Patil, D.; Singla, M.; Li, H.; Mo, Y.L.; Song, G. Parametric study of pounding tuned mass damper for subsea jumpers. *Smart Mater. Struct.* **2015**, *25*, 015028. [CrossRef]
82. Nguyen, X.-T.; Miura, N.; Nguyen, V.-T.; Bui, T.-L. Design of multiple tuned mass damper devices and application to response control of bridge under external force. *Mech. Based Des. Struct. Mach.* **2021**, 1–18. [CrossRef]
83. Yin, X.; Liu, Y.; Song, G.; Mo, Y.L. Suppression of bridge vibration induced by moving vehicles using pounding tuned mass dampers. *J. Bridg. Eng.* **2018**, *23*, 1–14. [CrossRef]
84. Wang, W.; Hua, X. Modeling, simulation, and validation of a pendulum-pounding tuned mass damper for vibration control. *Struct. Control. Health Monit.* **2019**, *26*, e2326. [CrossRef]
85. Chapain, S.; Aly, A.M. Vibration Attenuation in Wind Turbines: A Proposed Robust Pendulum Pounding TMD. *Eng. Struct.* **2021**, *233*, 111891. [CrossRef]
86. Jankowski, R. pounding force response spectrum under earthquake excitation. *Eng. Struct.* **2006**, *28*, 1149–1161. [CrossRef]
87. Muthukumar, S.; DesRoches, R. A Hertz contact model with nonlinear damping for pounding simulation. *Earthq. Eng. Struct. Dyn.* **2006**, *35*, 811–828. [CrossRef]
88. Ye, K.; Li, L.; Zhu, H. A modified Kelvin impact model for pounding simulation of base-isolated building with adjacent structures. *Earthq. Eng. Struct. Dyn.* **2009**, *8*, 433–446. [CrossRef]
89. Maison, B.F.; Kasai, K. Dynamics of pounding when two buildings collide. *Earthq. Eng. Struct. Dyn.* **1992**, *21*, 771–786. [CrossRef]
90. Jankowski, R. Nonlinear viscoelastic modelling of earthquake-induced structural pounding. *Earthq. Eng. Struct. Dyn.* **2005**, *34*, 595–611. [CrossRef]
91. Pratesi, F.; Sorace, S.; Terenzi, G. Analysis and mitigation of seismic pounding of a slender R/C bell tower. *Eng. Struct.* **2014**, *71*, 23–34. [CrossRef]
92. PEER. Strong Ground Motion Databases. 2021. Available online: <https://peer.berkeley.edu/peer-strong-ground-motion-databases> (accessed on 4 February 2023).
93. International Code Council. *Vol 2—Structural Engineering Design Provisions*; International Conference of Building Officials: Whittier, CA, USA, 1997.
94. Raheem, S. Seismic pounding between adjacent building structures. *Electron. J. Struct. Eng.* **2006**, *6*, 66–74. Available online: <http://www.ejse.org/Archives/Fulltext/2006/200608.pdf> (accessed on 4 February 2023).
95. Park, S.H.; Lee, P.J. Effects of floor impact noise on psychophysiological responses. *Build. Environ.* **2017**, *116*, 173–181. [CrossRef]
96. Akay, A. A review of impact noise. *J. Acoust. Soc. Am.* **1978**, *64*, 977–987. [CrossRef]
97. Tandon, N. Noise-reducing designs of machines and structures. *Sadhana-Acad. Proc. Eng. Sci.* **2000**, *25*, 331–339. [CrossRef]

Disclaimer/Publisher’s Note: The statements, opinions and data contained in all publications are solely those of the individual author(s) and contributor(s) and not of MDPI and/or the editor(s). MDPI and/or the editor(s) disclaim responsibility for any injury to people or property resulting from any ideas, methods, instructions or products referred to in the content.